https://doi.org/10.5194/egusphere-2026-5253
Preprint. Discussion started: 11 September 2026

Long-term climatic and management drivers of cropland gross primary production (GPP) from eddy covariance explained by interpretable machine learning

Sarah Maxwell[1], Fabio Turco[1], Yi Wang[1,2], Lukas Hörtnagl[1], Nina Buchmann[1], and Flavian Tschurr[1*]

[1]Grassland Sciences Group, Institute of Agricultural Sciences, ETH Zurich, Switzerland
[2]ICOS ERIC Carbon Portal, Department of Earth and Environmental Sciences, Lund University, 22362 Lund, Sweden
[*]Corresponding author. Email: flavian.tschurr@usys.ethz.ch

https://doi.org/10.5194/egusphere-2026-5253
Preprint. Discussion started: 11 September 2026

Abstract

Understanding the long-term response of cropland gross primary production (GPP) to climate variability remains limited, despite the key role of agricultural carbon fluxes in climate change mitigation. Here, we analyze two decades of eddy covariance measurements from a Swiss cropland site to assess how climate and management influence GPP dynamics of three winter crops: wheat, barley, and rapeseed. Crop-specific growing seasons were characterized by fitting logistic functions to cumulative GPP as a function of growing degree days, allowing the extraction of phenological metrics and growth rates. In parallel, an eXtreme Gradient Boosting (XGBoost) model combined with SHapley Additive Explanations (SHAP) was used to identify the dominant climatic and management drivers of daily GPP and their temporal patterns.

Air temperature and vapor pressure deficit exhibited significant increasing trends over the study period, consistent with ongoing climate change. However, no corresponding trends were detected during either actual or fixed winter growing season (October–July). Instead, significant warming and atmospheric drying were determined to occur during the post-harvest off-season (August–September). This shows that a crop rotation dominated by winter crops acts as a climate-smart strategy for the Oensingen site, enabling crops to escape intensifying peak summer heat and atmospheric dryness. Across crops, cumulative GPP trajectories and growth rates were largely similar. Winter wheat was the only crop showing a significant increase in maximum cumulative GPP over time, yet this increase was not reflected in grain yield, confirming that GPP is a poor predictor of harvested production. Machine-learning results identified incoming radiation, air temperature, and nitrogen fertilization as the dominant drivers of GPP, highlighting the importance of explicitly accounting for management variables in cropland carbon flux studies.

Overall, the absence of strong crop-specific divergence and limiting responses suggests that the studied crops have not yet experienced climatically constraining conditions for carbon uptake. These findings emphasize the need for long-term, multi-site cropland observations that integrate management data to better assess crop-climate interactions under future climate change.

https://doi.org/10.5194/egusphere-2026-5253
Preprint. Discussion started: 11 September 2026

1 Introduction

Agricultural land use is a dominant part of the terrestrial biosphere, accounting for approximately 38% of the total global land area, of which croplands represent about 12% (FAO 2023). Croplands, in particular, contribute substantially to regional carbon (C) budgets through plant productivity, soil organic matter dynamics, and management-driven C exports via harvest, or inputs via organic fertilization (Schmidt et al. 2012; Ceschia et al. 2010). Cropland ecosystems are very important but remain highly variable in their net C balance and may function either as C sinks or sources depending on climate conditions, crop type, and management practices (Emmel et al. 2018; Zhang et al. 2020). In contrast to forest and grassland ecosystems, whose long-term carbon dynamics have been extensively studied (Bonan 2008; Schils et al. 2022; Wang et al. 2026), croplands remain comparatively underrepresented in ecosystem-scale flux research, particularly over multi-decadal timescales.

Gross primary production (GPP), defined as the total uptake of atmospheric CO_2 through photosynthesis, represents the primary entry point of carbon into terrestrial ecosystems and provides a direct measure of vegetation productivity (Chen et al. 2021a). At the ecosystem scale, net carbon exchange with the atmosphere results from the balance between GPP and carbon losses through ecosystem respiration (Reco), which together determine the net ecosystem CO_2 exchange (NEE). In croplands, GPP is strongly influenced by climatic drivers such as radiation, temperature, vapor pressure deficit, and water availability, as well as by the crop type and management interventions such as fertilization (Li et al. 2024). Variations in GPP therefore reflect both short-term climate variability and longer-term shifts in growing conditions, making it a key variable for assessing climate sensitivity in agricultural systems (Anav et al. 2015).

Nevertheless, long-term analyses of cropland GPP remain scarce. Most existing cropland flux studies are limited to relatively short observation periods (Anthoni et al. 2004; Aubinet et al. 2009; Béziat et al. 2009; Moureaux et al. 2008), which restricts the ability to detect interannual variability, long-term trends, and climate-driven shifts in ecosystem functioning. Although some studies have investigated crop GPP over longer time spans (Buysse et al. 2017; Dold et al. 2017), the climatic drivers of cropland GPP and their potential shifts under ongoing climate change remain poorly constrained.

The global FLUXNET network provides eddy covariance (EC) observations of ecosystem-atmosphere CO_2 exchange, enabling detailed analyses of carbon flux dynamics across a wide range of ecosystems (Falge et al. 2002; Pastorello et al. 2020). However, only a limited number of cropland sites within FLUXNET offer long, continuous records spanning multiple decades. Such records are essential for disentangling long-term trends in GPP from short-term variability. Among these, the Oensingen cropland site in Switzerland, part of the SwissFluxNet (SwissFluxNet accessed 2026), provides one of the longest and most consistent cropland flux time series available. The high temporal resolution and extended coverage of this dataset provide a unique opportunity to examine how cropland GPP responds to climatic variability over a prolonged period. Nevertheless, isolating the respective effects of meteorological conditions, crop development, and management remains challenging due to non-linear responses and confounding interactions among drivers (Liu et al. 2024; Guevara-Escobar

https://doi.org/10.5194/egusphere-2026-5253
Preprint. Discussion started: 11 September 2026

et al. 2021).

Machine learning methods have increasingly been applied to ecosystem flux datasets to capture complex, non-linear relationships among climatic drivers (Pichler and Hartig 2023). In particular, gradient-boosting algorithms such as eXtreme Gradient Boosting (XGBoost) have demonstrated strong performance for GPP estimation (Borowiec et al. 2022; Cai et al. 2023). To enhance interpretability, SHapley Additive exPlanations (SHAP) can be used to quantify the contribution of individual climatic variables to model predictions (Chen et al. 2023a), thereby enabling a more process-oriented assessment of dominant GPP drivers and their temporal variability (Zhou et al. 2024). This framework enables attribution of observed GPP dynamics to specific drivers rather than relying solely on aggregated importance metrics (Krebs et al. 2025; Scapucci et al. 2024).

In this study, we analyze sixteen growing seasons of three winter crop types spanning two decades at a single FLUXNET cropland site to investigate the climatic drivers of GPP and their temporal dynamics. Specifically, we address the following research questions:

1. To what extent is climate change detectable in the long-term record of climatic variables at the site?

2. How have crop GPP patterns evolved across years, and are there systematic trends?

3. Which climatic and management variables exert the strongest influence on GPP, and how do their effects differ among crops?

To answer these questions, this study combines temporal trend analysis using regression models with the XGBoost-SHAP framework to assess the dominant climatic drivers of GPP and their temporal dynamics.

2 Methods

2.1 Site

The Oensingen site is located in the canton of Solothurn, Switzerland (47°17′11.1″ N, 7°44′01.5″ E; 452 m a.s.l.). The soil type is a Eutri-stagnic Cambisol and has a silty-clay texture (Hastings et al. 2010; Dietiker et al. 2010).

The site is a 1.55 hectare arable field and is managed according to an integrated farming label (IP Suisse). It represents an intensively managed cropland system dominated by winter crops. The crop rotation is centered on winter wheat, winter barley, and rapeseed, with winter wheat being the main crop. The crop rotation also alternates with peas, potatoes, and grass. In more recent years, cover crops have been sown between growing periods to prevent bare soil and are subsequently mulched into the soil (Table A.1).

2.2 Data collection and treatment

Since December 2003, eddy-covariance (EC) and meteorological data have been collected continuously at the Oensingen site (FLUXNET identifier: CH-Oe2) at high temporal resolution and are

https://doi.org/10.5194/egusphere-2026-5253
Preprint. Discussion started: 11 September 2026

available from FLUXNET (Buchmann et al. 2024). The EC tower is equipped with an infrared gas analyzer for measuring atmospheric CO_2 concentrations and an ultrasonic anemometer for determining three-dimensional wind speed and direction. This allows the calculation of turbulent CO_2 fluxes based on the covariance between vertical wind velocity and concentration fluctuations. In this study, we used the dataset processed, gapfilled, and filtered by FLUXNET (Buchmann et al. 2024).

The EC data are processed by FLUXNET and hence follow their processing pipeline (Pastorello et al. 2020). A quality control step applies a friction velocity (u*) filter, whereby only measurements above a threshold u* value are retained to exclude periods with insufficient turbulent mixing. Data gaps were filled using the Marginal Distribution Sampling (MDS) method (Reichstein et al. 2005; Papale et al. 2006; Pastorello et al. 2020). When gaps exceed the temporal limits of the MDS methods, missing meteorological values are supplemented from the ERA model, which provides a global gridded estimate for climatic variables (Balsamo et al. 2015). All processed data are assigned quality flags.

The EC technique directly measures net ecosystem exchange (NEE), which is the net exchange of all CO_2 fluxes between the atmosphere and the biosphere. NEE can be partitioned into ecosystem respiration (C loss) and gross primary production (C uptake; GPP). GPP is calculated using the nighttime partitioning method from Reichstein et al. (2005), in which nighttime NEE is assumed to represent total ecosystem respiration (including both soil and plant respiration). Respiration is modeled as a function of temperature and subtracted from daytime NEE to estimate GPP. The resulting half-hourly GPP values are aggregated into daily, monthly, and annual time series, yielding four levels of temporal aggregation. In the context of this study, only daily sum GPP (*GPP_NT_CUT_50*; in $\mathrm{g\,C\,m^{-2}\,d^{-1}}$) data are used for subsequent analyses.

Meteorological variables were also recorded at high temporal resolution and aggregated to half-hourly intervals. The measurements include air temperature (TA) (in °C), precipitation (P) (in mm), vapor pressure deficit (VPD) (in kPa) and incoming photosynthetic photon flux density (PPFD) (in μmol photons $\mathrm{m^{-2}s^{-1}}$). Precipitation was additionally transformed into the standardized precipitation index (SPI) to capture short-term moisture anomalies, using a 30-day running window. The SPI is a normally distributed, simplified water balance that represents water availability for the plants more realistically than raw daily precipitation values. It was calculated using the `SPEI` R package (Beguería and Vicente-Serrano 2023). Missing PPFD values have been gap-filled by using linear model based on short-wave radiation measurements. Meteorological data underwent the FLUXNET control and gap-filling procedures as the EC flux data, with missing values filled using the MDS approach or supplemented with ERA-Interim reanalysis data when necessary. For the subsequent analyses, climatic variables were primarily used at daily resolution. Yearly values were used for assessing temporal trends. In addition, daily values were aggregated as averages or sums (precipitation) over the growing period.

2.3 Management data

In addition to the flux and meteorological measurements, a comprehensive management dataset is available for the Oensingen site. This dataset is available as part of the SwissFluxNet (`https:`

https://doi.org/10.5194/egusphere-2026-5253
Preprint. Discussion started: 11 September 2026

`//www.swissfluxnet.ethz.ch/`) and includes key management events, such as sowing and harvest dates, mineral and organic fertilization (dates and applied nitrogen amounts), as well as grain and straw yields. The growing period for each crop was defined as the time span between the sowing and harvest dates derived from the management records. The days after sowing (DAS) were calculated by counting the number of days from the sowing date (DAS = 1) until harvest. The growing periods of winter wheat in 2004 and winter barley in 2023 were excluded from the trend analysis because they were not fully covered by the available flux and meteorological datasets.

Grain and straw yield (in kilograms per hectare) of winter wheat and winter barley were extracted from the management data. Based on these data, the harvest index was calculated as the proportion of grain yield relative to total aboveground biomass production (Eq. 1):

$$\text{Harvest index} = \frac{yield_{grain}}{yield_{grain} + yield_{straw}} \tag{1}$$

2.4 Temporal trends in climate or management practices

Temporal trends in climatic and management variables were assessed using linear and linear mixed-effects models. These complementary approaches allow for the evaluation of both crop-specific and overall trends across the study period.

For individual variables, linear regression models were applied to estimate temporal trends either for the entire dataset or separately for each crop type. In the crop-specific analyses, separate linear regression models were fitted for each crop to identify their trends.

To assess trends across all crops while accounting for crop-specific variability, linear mixed-effects models were used. In these models, the variable of interest (e.g., mean temperature during the growing period) was regressed on time, while crop type was included as a random effect to allow for different intercepts among crops. Mixed-effects models were implemented using the `lme4` package in R (Bates et al. 2015).

In all models, the dependent variable was either a climatic variable (e.g., temperature, precipitation, VPD, PPFD) or a management-derived growth parameter (e.g., DAS, harvest index), and the independent variable was a time-related predictor, typically the harvest year or the date of the relevant management event.

Additionally, to assess whether winter cropping serves as a viable adaptation strategy for avoiding adverse summer environmental conditions, we evaluated environmental covariate trends during a fixed growing season (October to July) versus the post-harvest off-season (August and September).

2.5 Extracting key timepoints of crop GPP dynamics

To facilitate the comparison of cumulative GPP curves across years, growth parameters were extracted, representing distinct physiological stages of crop development. Because cumulative GPP curves typically exhibit an S-shaped trajectory, three key parameters were defined:

1. **Start of the growing period**: start of season (SOS) is defined as the time point at which the crop initiates vegetative growth and begins substantial carbon assimilation for biomass

https://doi.org/10.5194/egusphere-2026-5253
Preprint. Discussion started: 11 September 2026

accumulation.

2. **End of the growing period**: end of season (EOS) is defined as the time point at which GPP accumulation decreases as the crop reaches maturity and vegetative growth ceases.

3. **Length of the growing season**: The period between SOS and EOS.

SOS and EOS were defined as the transition points of the fitted cumulative GPP curves. Specifically, the start of the period corresponds to 50% of the maximum of the second derivative (accelerating phase) prior to the maximum, and the end corresponds to 50% of the minimum of the second derivative (decelerating phase) after the minimum, as similarly done in Tschurr et al. 2024. For clarity, the period between these transition points is referred to as the *main growing period*, which differs from the full growing period defined from sowing to harvest.

Cumulative GPP curves were more symmetrical when plotted against thermal time rather than calendar days. Therefore, GPP was fitted against growing degree days (growing degree days (GDD)) using the logistic model implemented in the `nlsLM()` function from the `minpack.lm` package in R (Elzhov et al. 2023). GDD was calculated from daily mean temperature (T_{mean}) with a base temperature of 0 °C (T_{base}) as (Eq. 2):

$$\mathrm{GDD} \;=\; \sum_{i=1}^{n} \max(0,\ T_{\mathrm{mean},i} - T_{\mathrm{base}}) \tag{2}$$

where n is the number of days of the cultivation period. To compare the GPP patterns of the crops over the years, the growth parameters extracted from the fitting were then used in a trend analysis as mentioned in the earlier section.

2.6 eXtreme Gradient Boosting modeling

To determine the dominant climatic drivers of daily GPP, an eXtreme Gradient Boosting (XGBoost) model was implemented using the `xgboost` package in R (Chen et al. 2023b). Daily GPP served as the response variable, while the predictor set included TA, VPD, PPFD, and SPI. Additionally, the amount of nitrogen (N) fertilization was used as a predictor in the model to account for management effects on crop productivity.

The temporal effect of fertilization in the model was represented by distributing the total amount of N evenly (i.e., each day with the same N value during the fertilization period) over a decay period until complete uptake, or the pre-fertilization condition, was assumed. Different decay durations were applied for mineral fertilizer (30 days) and manure (50 days), reflecting their contrasting release dynamics. These linear release rates were derived from Niedziński et al. (2021) and Xu et al. (2021).

The full dataset was split into a training set (70%) and a testing set (30%), selecting the fixed splitting ratio from each month of each cropping season randomly. Hyperparameter tuning was performed using a Bayesian optimization framework (Snoek et al. 2012; Wu et al. 2019), minimizing the mean absolute error (MAE) based on 5-fold cross-validation with equally sized folds. The algorithm randomly samples starting values inside the parameter bounds (Table A.7) and iteratively

https://doi.org/10.5194/egusphere-2026-5253
Preprint. Discussion started: 11 September 2026

explores the parameter space using an acquisition function (Wang et al. 2023b). The final optimized hyperparameter values are reported in the Appendix (Table A.8).

After tuning, the model was retrained using the optimized hyperparameters. Model performance was evaluated by comparing predicted and observed GPP values from the independent test set. Performance metrics included the (root mean square error (RMSE)), Pearson correlation coefficient, and (mean absolute error (MAE)).

Two modeling strategies were tested: a single model fitted across all crop types using the crop type as a factorial predictor and separate models fitted for each crop. As no substantial improvement in predictive ability was observed with crop-specific models (Table A.9), a single unified model was retained and used for subsequent analyses. This means the factor crop type will indicate whether, in general, lower GPP is predicted when one crop is grown compared to another.

Furthermore, we trained and tested the selected model with all crop types integrated as factorial variables for the whole season (sowing to harvest) and for the season from sowing to EOS. Physiologically, it is expected that maturity processes dominate the GPP after EOS, and not the environmental covariates as before. For subsequent analyses, the model, integrating all crop types, trained on data between sowing and EOS was used (Table A.9).

2.7 Gross primary production driver assessment using SHAP

It is important to acknowledge that the GPP variable used in this study is a derived product obtained through the nighttime partitioning algorithm, which explicitly relies on air temperature (TA) to model ecosystem respiration. Consequently, an inherent dependency exists between the derived GPP signal and temperature. However, the standard partitioning approach assumes a fixed functional response (e.g., the Lloyd-Taylor parameterization) parameterized over short time windows. In contrast, our XGBoost-SHAP framework is data-driven and free from such rigid functional constraints. This allows the model to identify complex, non-linear biological responses and interactions (e.g., temperature optima or varying sensitivities across phenological stages) that extend beyond the mathematical assumptions used to generate the GPP dataset. We furthermore run the following approach twice, using daytime and nighttime GPP partitioning methods as the target variable while keeping the rest of the analysis equal. We then correlated the SHAP values between daytime and nighttime-partitioned GPP.

To investigate how the relative importance of climatic and management drivers of GPP varied over time, a SHapley Additive exPlanations (SHAP) analysis was applied to the whole dataset. SHAP is a game-theory-based approach that explains individual model predictions by quantifying the contribution of each predictor variable to the output of the XGBoost model. Therefore, it allows for the decomposition of each model prediction into additive contributions from the input variables (Lundberg and Lee 2017; Chen et al. 2023a).

For each daily prediction, the SHAP values indicate how much a given driver increases or decreases the predicted GPP relative to the model's baseline prediction. The baseline is defined as the mean GPP across the training dataset and represents the expected model prediction in the absence of specific information about the predictor variables. Positive SHAP values indicate that a

https://doi.org/10.5194/egusphere-2026-5253
Preprint. Discussion started: 11 September 2026

driver increases predicted GPP above the baseline, whereas negative values indicate a reduction in predicted GPP. By aggregating SHAP values across time, it is possible to identify both short-term seasonal patterns and longer-term shifts in the dominant controls on GPP.

This framework enables the analysis of seasonal patterns and temporal shifts in the influence of individual meteorological and management drivers on GPP. SHAP values were computed using the `SHAPforxgboost` package in R (Liu and Just 2023).

3 Results

3.1 Temperature increases over the study period

All climatic variables exhibited a pronounced seasonal pattern, with higher values in summer than in winter, except precipitation, which showed no clear seasonal trend (Figure A.1). Over the entire study period, the mean annual air temperature was 9.9 °C, and the average annual precipitation was 1132 mm. Both VPD and air temperature increased significantly over the study period, although both variables also showed substantial scatter around these trends, (Figure 1), whereas PPFD and precipitation did not exhibit consistent temporal trends. In particular, the temperature increased at a rate of 0.06 °C per year (p-value = 0.02) (Table A.2).

https://doi.org/10.5194/egusphere-2026-5253
Preprint. Discussion started: 11 September 2026

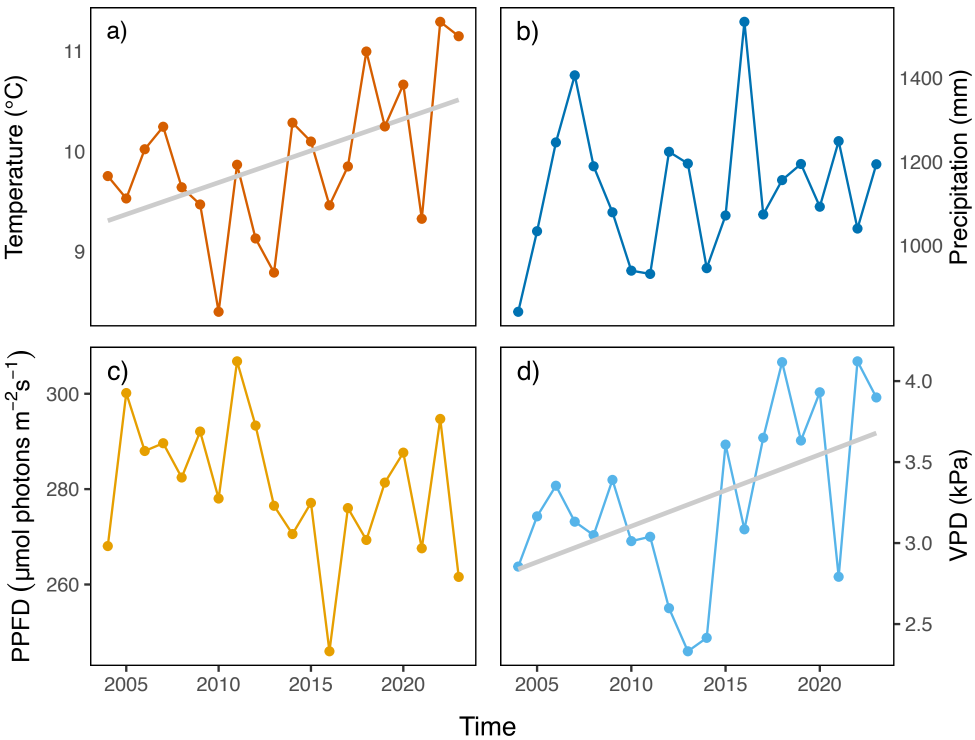

Figure 1: Trends in annually aggregated climatic variables over the study period. Temperature (°C) (a), incoming photosynthetic photon flux density (PPFD; μmol photons $m^{-2}s^{-1}$) (c), and vapor pressure deficit (VPD; kPa) (d) are shown as annual means, while precipitation (mm) (b) is shown as an annual sum. Grey regression lines indicate statistically significant trends from the linear model ($p < 0.05$).

However, when climatic variables were averaged across each crop growing season, no significant temporal trends were detected for temperature, VPD, or precipitation, either for each crop separately or for all crops combined (Figure 2, Table A.3). Likewise, sowing and harvest dates did not exhibit clear long-term trends (Figure 2). Nevertheless, the linear mixed-effect models indicated a slight shift toward earlier harvest dates, with an average advance of approximately half a day per year (p-value=0.03), following a corresponding shortening of the growing season (sowing to harvest) length (p-value = 0.07) (Table A.4).

https://doi.org/10.5194/egusphere-2026-5253
Preprint. Discussion started: 11 September 2026

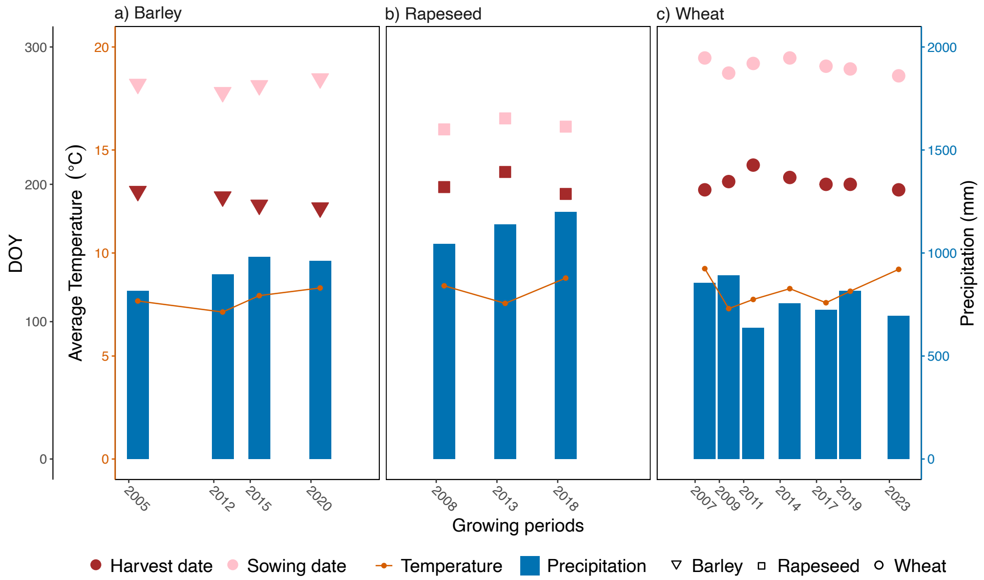

Figure 2: Average Temperature (orange line) and total precipitation (blue bars) during the growing periods of winter barley (a), rapeseed (b), and winter wheat (c). Temperature is shown on the left y-axis, and precipitation on the right y-axis. Sowing and harvest dates (in DOY) are indicated in pink and dark violet, respectively, aligned with the outer left y-axis.

Analyzing the fixed climatological windows revealed a clear contrast between the growing season and the post-harvest off-season. Within the fixed growing season (October to July), environmental covariates remained stable, showing no significant long-term trends for air temperature, VPD, or precipitation ($p > 0.70$; Table A.5); the only exception was a significant decline in PPFD (slope $= -3.81$,µmol,$\mathrm{m^{-2}\,s^{-1}}$ per year, $p = 0.005$). In clear contrast, the post-harvest off-season (August and September) experienced pronounced warming and atmospheric drying, marked by significant increases in both VPD (slope $= +0.13$ kPa, $p = 0.003$) and air temperature (slope $= +0.08$ °C, $p = 0.035$). Off-season precipitation and PPFD showed no significant shifts ($p = 0.21$ and $p = 0.62$, respectively).

3.2 Seasonal cumulative GPP increases over the years in winter wheat

Across the study period, of seven complete growing seasons, winter wheat exhibited the highest mean daily GPP 5.1 $\mathrm{g\,C\,m^{-2}\,d^{-1}}$, followed by winter barley with an average of 4.2 $\mathrm{g\,C\,m^{-2}\,d^{-1}}$ over four complete growing seasons, and rapeseed with an average of 4.1 $\mathrm{g\,C\,m^{-2}\,d^{-1}}$ over three growing seasons. Among the three crops, wheat also reached the highest daily GPP values (Figure 3).

https://doi.org/10.5194/egusphere-2026-5253
Preprint. Discussion started: 11 September 2026

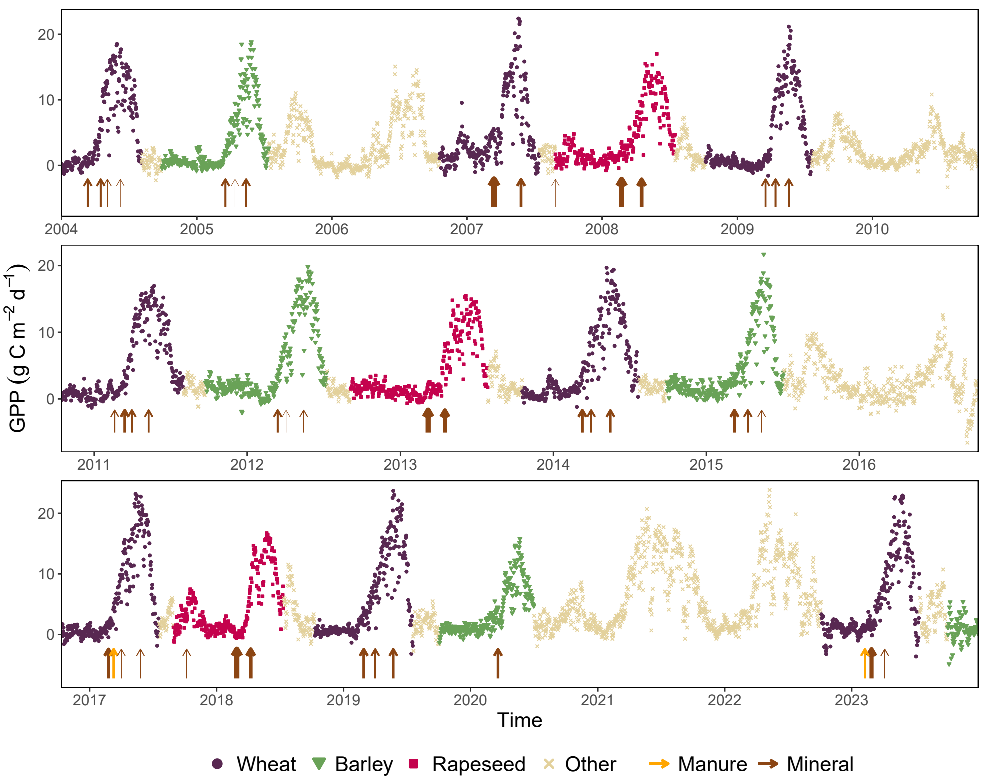

Figure 3: Daily values of gross primary production (GPP; $g\,C\,m^{-2}\,d^{-1}$) over the study period. Arrows indicate the timing of fertilization events during the cultivation of winter wheat, winter barley, and rapeseed, with arrow width proportional to the applied nitrogen amount (ranging from 17.5 to $90\,kg\,N\,ha^{-1}$) (see table A.1 for seasonal N input information).

Seasonal cumulative GPP followed an asymmetric logistic trajectory when plotted against days after sowing, characterized by a prolonged initial phase associated with winter dormancy, followed by a rapid increase during spring growth and a plateau towards crop maturity (Figure 4). Across all crops, carbon uptake remained low during the colder winter period (November to March), reflecting reduced photosynthetic activity, before accelerating as temperature and PPFD increased. No prolonged maturity phase could be measured, as the farmer harvests the crops as soon as the GPP intake reaches a plateau, which is linked to physiological maturity. Among the three crops, winter wheat showed the highest seasonal cumulative GPP, with a mean of $1435\,g\,C\,m^{-2}$, followed by rapeseed ($1337\,g\,C\,m^{-2}$) and winter barley ($1177\,g\,C\,m^{-2}$). A significant positive trend across the years was detected in the maximum seasonal cumulative GPP of winter wheat ($p = 0.04$), corresponding to an average increase of $21.9\,g\,C\,m^{-2}$. In contrast, no significant trends were observed for winter barley or rapeseed, nor in the pooled analysis across all crops.

https://doi.org/10.5194/egusphere-2026-5253
Preprint. Discussion started: 11 September 2026

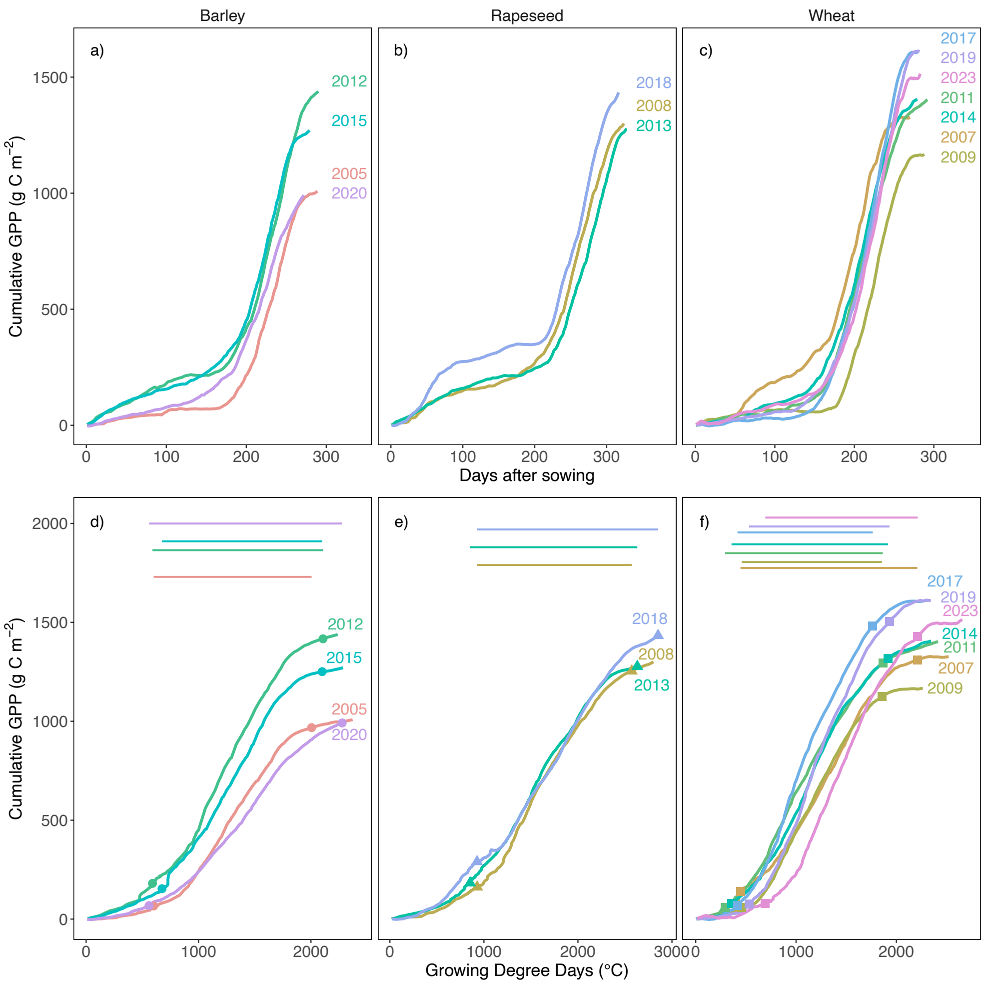

Figure 4: Cumulative gross primary production (GPP; g C m^{-2}) during the growing period for winter barley (a, d), rapeseed (b, e), and winter wheat (c, f). The x-axis represents days after sowing (a–c) or growing degree days (d–f). The harvest year of each growing period is indicated to the right of each curve. Points mark the start (SOS) and end (EOS) of the main growing period (see Section 2.5), and colored bars indicate growing season length (d-f).

Overall, no trend is apparent across the three crops regarding their SOS, EOS, or growing season length. We observed a significant extension of the growing season length of winter barley and a delayed EOS. Rapeseed also showed a significant increase in the length of the growing period due to an earlier start of the main growing season. However, as the trends for rapeseed and winter barley are only based on four or fewer growing seasons, they will not be discussed further.

https://doi.org/10.5194/egusphere-2026-5253
Preprint. Discussion started: 11 September 2026

3.3 GPP does not correlate with grain yield

For winter wheat and winter barley combined, the seasonal cumulative GPP showed a significant correlation with total yield and harvest index, but not with grain yield (Figure 5). Specifically, an increase of 1 $g\,C\,m^{-2}$ in the cumulative GPP was associated with an increase of 5.7 $kg\,ha^{-1}$ in straw yield (p-value = 0.006). In contrast, no significant relationship was detected between cumulative GPP and grain yield for either crop. Moreover, the harvest index decreased significantly with increasing cumulative GPP ($p = 0.02$). As a result, while total biomass increased with higher GPP, the ratio of assimilated carbon allocated to grain decreased (Figure 5b and Table A.6).

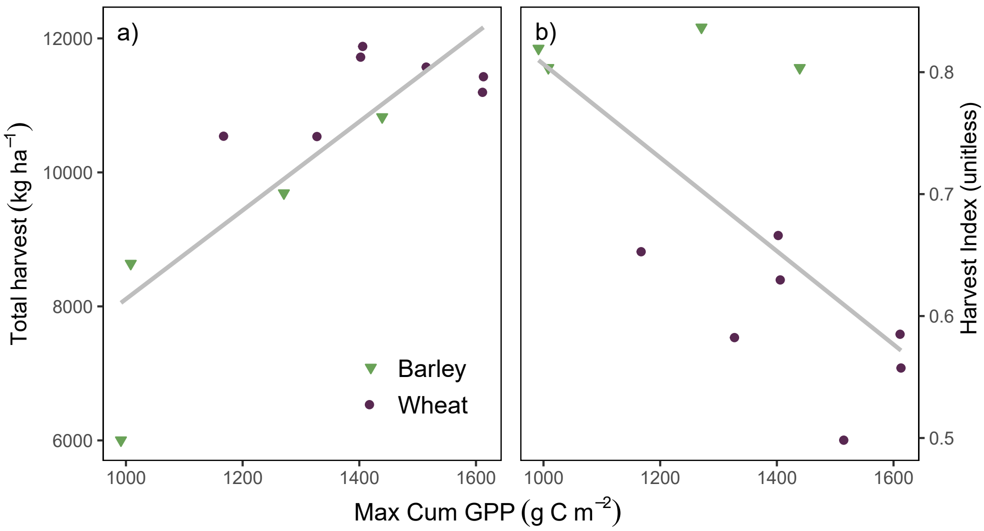

Figure 5: Grain and straw yield responses to maximum cumulative gross primary production over the growing period (GPP; $g\,C\,m^{-2}$) for winter wheat (purple) and winter barley (green): total yield ($kg\ ha^{-1}$) (a), and harvest index (unitless) (b). The grey lines indicate statistically significant relationships ($p < 0.05$) of a linear model combining both crop types (see Table A.6).

3.4 GPP's main drivers are Temperature and PPFD

The XGBoost model demonstrated high predictive accuracy on the independent test set, with a Pearson correlation coefficient (r) of 0.92 (r^2=0.85). Model performance metrics indicated a RMSE of 2.23 and a MAE of 0.11 $g\,C\,m^{-2}\,d^{-1}$ (Table A.9). Temperature and PPFD were the main drivers of GPP with substantially higher SHAP contributions than the other variables (Figure A.2).

Correlation between daytime- and nighttime-partitioned GPP was high for the important drivers. The RMSE remained small for all predictors (below 0.77) (Figure A.4), suggesting that this approach is stable across different partitioning methods.

The SHAP response curves illustrate the marginal effects of each predictor on GPP, isolated from interactions with other variables (Figure 6). PPFD shows a near-linear positive relationship

https://doi.org/10.5194/egusphere-2026-5253
Preprint. Discussion started: 11 September 2026

with GPP until saturation occurred at approximately 600 µmol photons $m^{-2}\,s^{-1}$). In contrast, the temperature response exhibited a clear optimum around 15°C, beyond which SHAP values declined. Temperatures below 10°C or exceeding 20°C were associated with negative SHAP values, indicating reduced GPP relative to the model baseline. Fertilization also displayed a non-linear response, with positive contributions at moderate N levels and decreasing effects at higher application rates.

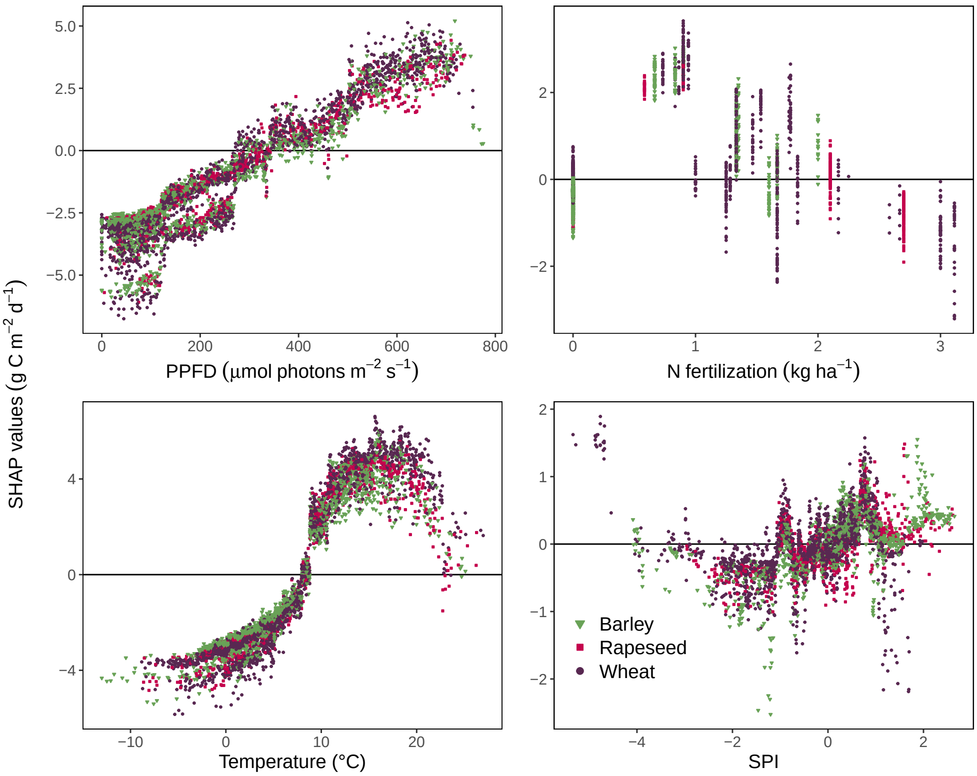

Figure 6: Response curves of the SHAP values (y-axis) for radiation (PPFD; μmol photons $m^{-2}s^{-1}$) (a), N fertilization (kg ha^{-1}) (b), temperature (°C) (c), and standardized precipitation index (SPI; unitless) (d) as a function of the observed predictor values (x-axis) for winter wheat, winter barley, and rapeseed. Negative SHAP values indicate a negative contribution to the predicted gross primary production (GPP) from the mean prediction/baseline prediction, while a positive value indicates a positive contribution from the mean 6.55 g C m^{-2} d^{-1}.

Seasonal patterns in driver importance were consistent across crops and years. At the beginning of spring, SHAP values for both temperature and PPFD shifted from negative to positive, reflecting the transition from the winter period to the active growth phase (Figure 7, 8, and 9). Toward the end of the growing period for winter barley and rapeseed, fertilization's SHAP values tend to shift from positive to negative. Some peculiar cases are winter wheat grown in 2007 and winter barley grown in 2020, where fertilization nearly always has a negative SHAP value, corresponding to years

https://doi.org/10.5194/egusphere-2026-5253
Preprint. Discussion started: 11 September 2026

when barley and wheat were less frequently fertilized than in other growing periods (Figure 3). Notably, winter barley in 2020 also showed the lowest cumulative GPP among all barley growing periods (Figure 4a), highlighting the interaction between management intensity and carbon uptake.

The crop type also has a relatively constant but important effect on GPP prediction, with winter wheat consistently showing a higher SHAP value than the other two crops. However, across all three crops and across different growing periods, the SHAP values show a similar pattern, and their importance does not increase or decrease over the years. Only the contribution of PPFD showed a significant decline over time ($p = 0.005$), whereas the effects of temperature, fertilization, VPD, and SPI remained constant. The baseline of the model for the calculation of the SHAP values is equal to a GPP of $6.55\,\mathrm{g\,C\,m^{-2}\,d^{-1}}$

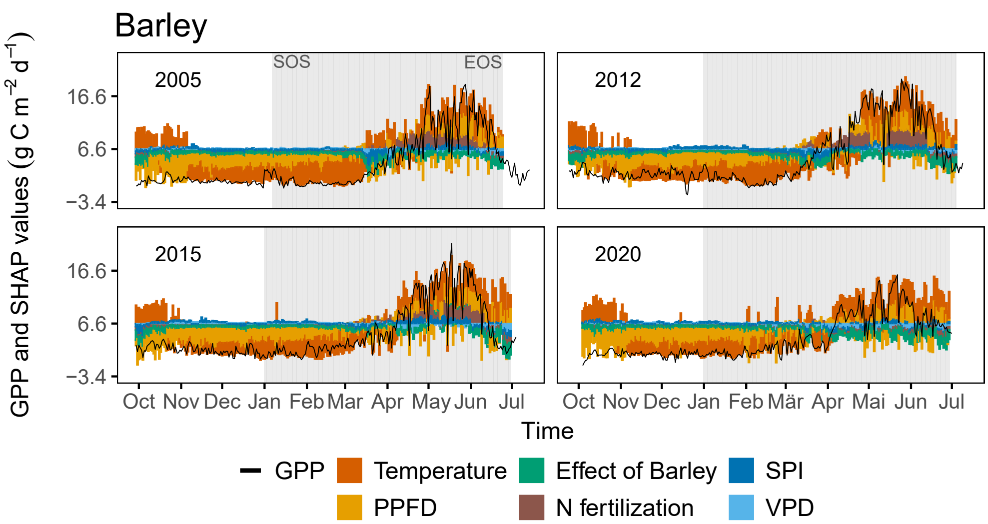

Figure 7: SHAP values and observed gross primary production (GPP; $\mathrm{g\,C\,m^{-2}\,d^{-1}}$) for the four growing periods of winter barley. Observed GPP is shown as a black line (from sowing to harvest), while daily SHAP values for each predictor are displayed as stacked bars relative to the model baseline (from sowing to the end of the season (EOS), according to the period to train the XGBoost model). Colors indicate individual predictors (PPFD, temperature, N fertilization, VPD, SPI, and the effect of barley). The baseline of the SHAP calculation equals $6.55\,\mathrm{g\,C\,m^{-2}\,d^{-1}}$. For each daily value, the sum of the baseline and all SHAP values yields the predicted GPP. The grey shape indicates the growing period between the defined start (SOS) and the end of the season (EOS).

https://doi.org/10.5194/egusphere-2026-5253
Preprint. Discussion started: 11 September 2026

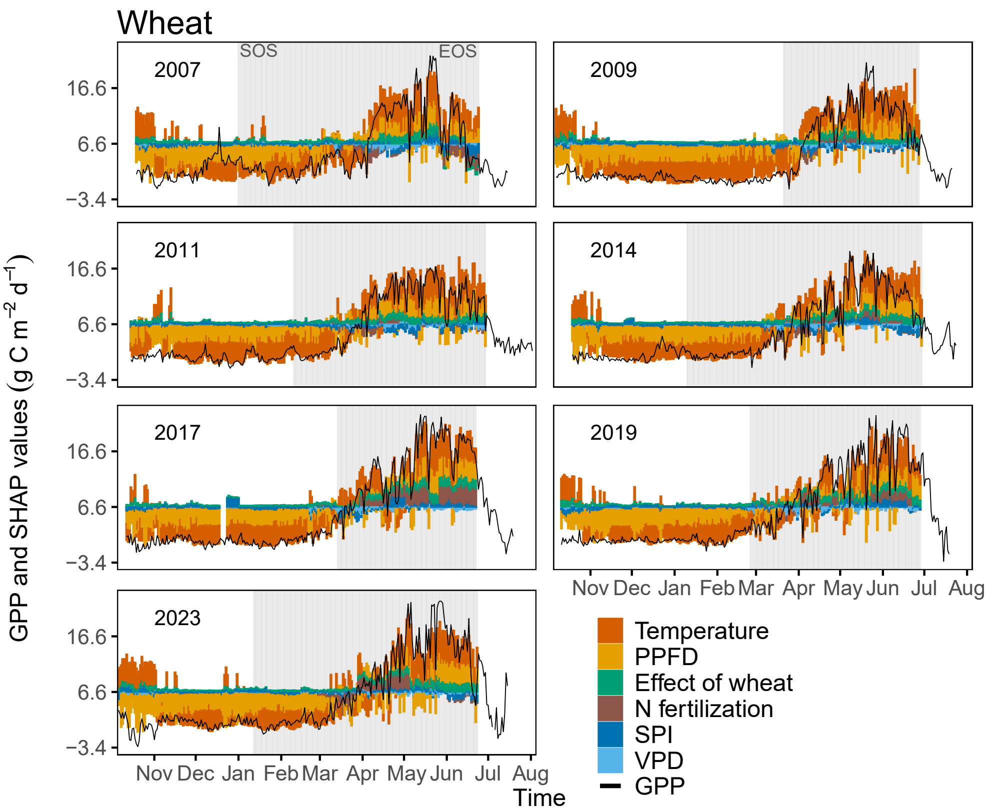

Figure 8: SHAP values and observed gross primary production (GPP; $\mathrm{g\,C\,m^{-2}\,d^{-1}}$) for the seven growing periods of winter wheat. Observed GPP is shown as a black line (from sowing to harvest), while daily SHAP values for each predictor are displayed as stacked bars relative to the model baseline (from sowing to the end of the season (EOS), according to the period to train the XGBoost model). Colors indicate individual predictors (PPFD, temperature, N fertilization, VPD, SPI, and the effect of wheat). The baseline of the SHAP calculation equals $6.55\,\mathrm{g\,C\,m^{-2}\,d^{-1}}$. For each daily value, the sum of the baseline and all positive and negative SHAP values yields the predicted GPP. The grey shape indicates the growing period between the defined start (SOS) and the end of the season (EOS).

https://doi.org/10.5194/egusphere-2026-5253
Preprint. Discussion started: 11 September 2026

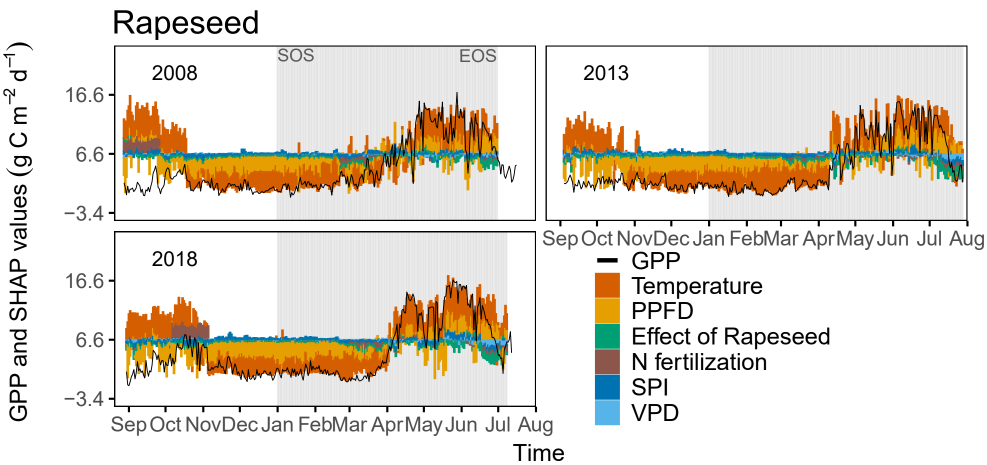

Figure 9: SHAP values and observed gross primary production (GPP; $\mathrm{g\,C\,m^{-2}\,d^{-1}}$) for the three growing periods of rapeseed. Observed GPP is shown as a black line (from sowing to harvest), while daily SHAP values for each predictor are displayed as stacked bars relative to the model baseline (from sowing to the end of the season (EOS), according to the period to train the XGBoost model). Colors indicate individual predictors (PPFD, temperature, N fertilization, VPD, SPI, and the effect of rapeseed). The baseline of the SHAP calculation equals $6.55\,\mathrm{g\,C\,m^{-2}\,d^{-1}}$. For each daily value, the sum of the baseline and all positive and negative SHAP values yields the predicted GPP. The grey shape indicates the growing period between the defined start (SOS) and the end of the season (EOS).

4 Discussion

4.1 Detectability of climate change in climatic variables

Climate change is detectable in the dataset when climatic variables are examined at different temporal resolutions. Air temperature and VPD significantly increased over the study period (Figure 1), with an increase of 0.06 degrees per year for temperature, consistent with climate warming scenarios for Switzerland (MeteoSwiss and Zurich 2025). In contrast, this warming trend was absent when examining the actual crop growing seasons based on sowing and harvest dates. Similarly, no significant trends were detected when evaluating a fixed growing season window from October to July (Table A.5). Instead, significant increases in temperature and VPD were isolated strictly to the post-harvest off-season (August and September). These contrasting seasonal dynamics indicate that prioritizing winter crops in the crop rotation represents an effective climate-smart management strategy for the Oensingen site, protecting the main growing period from intensifying summer heat and atmospheric dryness.

https://doi.org/10.5194/egusphere-2026-5253
Preprint. Discussion started: 11 September 2026

4.2 Long-term evolution of crop GPP patterns

Winter wheat exhibited a significant increase in season cumulative GPP over time. This increase was not accompanied by higher grain yields but was strongly associated with increased total biomass production, indicating preferential carbon allocation to vegetative biomass (Figure 5) (Suyker et al. 2005). This is also consistent with previous studies that found GPP as a poor predictor for grain yield (Buysse et al. 2017; Liu et al. 2023). This inverse relationship between grain yield and GPP is also supported by larger-scale research: while studies found that GPP increased globally (Lu et al. 2024; Zhang et al. 2019), others established that wheat grain production was expected to decline due to climate change (Asseng et al. 2015; Supit et al. 2010).

Cumulative GPP curves were similar across crops, particularly in terms of growth rates during the main growing period, suggesting that crops assimilate carbon at comparable maximum rates once favorable conditions are met (Figure 4). A slight phenological shift was observed, with a shortening of the main growing period and a later SOS in winter wheat. These patterns are consistent with climate change-driven phenological changes (Trnka et al. 2014; Le Roux et al. 2024; Xiao et al. 2013).

4.3 Climatic and management drivers of GPP

The XGBoost model accurately predicted the ecosystem's dynamic of GPP based on the climatic and management variables. The model performed with a high correlation (0.92), and a low MAE ($0.11\,\mathrm{g\,C\,m^{-2}\,d^{-1}}$). The RMSE of the model ($2.23\,\mathrm{g\,C\,m^{-2}\,d^{-1}}$) lies within the range reported in previous studies that estimated GPP with XGBoost modeling (Wang et al. 2023a; Menefee et al. 2023).

PPFD, temperature, and N fertilization were identified as the main drivers of GPP, while water-related variables played a minor role due to the relatively high precipitation at the site and the soil type, which is characterized by good fertility and periodic water stagnation, which can influence biogeochemical processes relevant for carbon cycling. In other studies focusing on GPP and climate interactions, PPFD and temperature were frequently found to be the main drivers on sites where water is not limiting (Chen et al. 2021b; Zhao et al. 2024; Eichelmann et al. 2016). We did not consider a potential CO_2 fertilization effect in the drivers analysis of this single-site study. However, it was determined that CO_2 could exert a substantial and beneficial influence on long-term GPP trend, thereby becoming a significant factor in the broader ecological context (Deryng et al. 2014; Zhu et al. 2016; Chen et al. 2021a), especially in multi-site analyses where different CO_2 levels and gradients are expected. Nevertheless, the N fertilization effect was taken into account in the analysis, which is often neglected in such models. The expected effect of N fertilization on GPP is to increase in importance (more positive SHAP value) with higher N fertilization rates. Our analysis revealed an unexpected partial dependency of N fertilization on GPP, showing the opposite trend (Figure 6). This may reflect the intrinsic simplification of our N fertilization descriptor, as it captures neither the long-term effects of fertilization nor the highly dynamic and unpredictable release of mineral N. Nevertheless, it was found to be the third most important factor of GPP assimilation, thus underscoring the importance of integrating management variables into drivers' assessments of

https://doi.org/10.5194/egusphere-2026-5253
Preprint. Discussion started: 11 September 2026

carbon fluxes.

The SHAP analysis revealed an optimum temperature for daily carbon fixation of ∼15°C (Figure 6c). This is a relatively low temperature optimum compared to previously reported values (Huang et al. 2019; Bennett et al. 2021; Pan et al. 2024), but this may be attributed to the adoption of cultivars optimized for the temperate climate of Switzerland as well as to a potential interaction with crop phenology (lower GPP during late stages). Daily temperature values over ∼20°C were found to have negative SHAP values (Figure 6c), hence a negative effect on crop GPP. This finding aligns with the observations documented in Porter and Gawith (1999) and Bernacchi et al. (2001). GPP is thus limited by temperature exceeding 20°C. Similarly, temperatures below 10°C are associated with negative SHAP values, indicating that an increase in the seasonal mean temperature can lead to higher overall GPP as long as temperatures remain below 20°C, given that the overall growing conditions are suitable, i.e., no drought period.

Despite the observed increase in temperature and VPD over the study period (Figure 1), there is no clear evidence that crops at the Oensingen site have already faced severe climatically limiting conditions for GPP. Winter wheat even exhibited a significant increase in cumulative GPP over time (Figure 4), while average growing-season temperatures for all crops remained below the threshold of 20°C identified as limiting in the SHAP analysis (Figure 6c). These results suggest that crop carbon assimilation at this site remains within a favorable climatic range and that the cultivated crops remain well adapted to the current climate, consistent with previous findings for Switzerland (Holzkämper et al. 2015). However, the analysis is based on mean daily values, whereas extreme events may occur at even shorter temporal resolutions and be smoothed out by averaging over a daily course. Also, aggregating half-hourly data to daily values introduces a temporal mismatch. Daily GPP reflects daytime photosynthesis, whereas temperature, VPD, and SPI are averaged over 24 hours, including nighttime conditions that do not drive GPP and may dilute predictor signals and slightly affect model performance.

However, an important source of uncertainty relates to management and cultivar changes over time. The relative stability observed in both GPP dynamics and SHAP values may partly reflect changes in the chosen crop cultivar, which has been shown to offset or mask climate-driven changes in crop phenology and productivity (Rezaei et al. 2018; Liu et al. 2018). We did not specifically address the effect of the specific cultivar, as not enough growing seasons are available to disentangle its effects. However, breeding progress and hence cultivar choice may have influenced the measured GPP.

Finally, the limited number of growing periods available per crop constrains the robustness of crop-specific trend detection, particularly for winter barley and rapeseed. While the Oensingen site provides a uniquely long cropland flux record, single-site analyses remain naturally limited in their ability to generalize crop responses to climate variability. This limitation motivates the need for broader, multi-site approaches.

https://doi.org/10.5194/egusphere-2026-5253
Preprint. Discussion started: 11 September 2026

5 Conclusions

Although FLUXNET has traditionally focused on forest and grassland ecosystems, this study highlights the need for more long-term cropland observations. Using two decades of eddy covariance measurements at a Swiss cropland site, we found no strong evidence that the studied winter crops have yet experienced climatically limiting conditions for gross primary production. Despite clear warming trends in temperature and atmospheric dryness, crop GPP remained stable across years, with a significant increase observed only for the cumulative GPP in winter wheat.

By explicitly integrating management information into the analysis, this study demonstrates that management, in this case nitrogen fertilization, sowing and harvest date, plays a key role in shaping cropland GPP, alongside climatic drivers such as temperature and radiation. The importance of management variables underscores the need to routinely include detailed management data in ecosystem-scale carbon flux analyses. However, such information is still rarely available in standardized flux datasets, which would allow for assessing management-climate interactions in a broader scope.

Although the dataset spans twenty years, it did not capture intense climatic extremes sufficiently to constrain crop GPP, highlighting a limitation of single-site studies. Future research should therefore rely on multi-site cropland networks and explicitly target extreme events rather than seasonal mean conditions. Expanding long-term, well-documented cropland flux observations – including management practices – is essential to improve understanding of crop carbon dynamics under ongoing climate change.

Acknowledgments

We thank the farmers Samuel Tschumi, Daniel and Walter Ingold for the management of the field and for providing information on the management. We greatly acknowledge the great work of all involved technicians (Peter Plüss, Thomas Baur, Philip Meier, Florian Kaeslin, Patrick Koller, Ivo Beck, Paul Linwood, Markus Staudinger, Martin Rüegg, Peter Ravelhofer). We further thank Carmen Emmel, Regine Maier, and all the previous site responsible persons of the CH-Oe2 site.

During the preparation of this work, the authors used Gemini, Grammarly, and NotebookLM to edit text for clarity and grammar, as well as to assist with coding scripts for figure generation. All AI-assisted code and text were thoroughly reviewed, tested, and validated by the authors, who take full responsibility for the final content and scientific interpretations of this publication.

Financial support

This work has received funding from the Swiss State Secretariat for Education, Research and Innovation (SERI), directed by the project NextGenCarbon (grant number 101184989).

https://doi.org/10.5194/egusphere-2026-5253
Preprint. Discussion started: 11 September 2026

Author contribution

SM: Conceptualization, Methodology, Formal analysis, Investigation, Visualization, Writing – original draft. FTu: Data curation, Resources, Writing – review & editing. YW: Data curation, Resources, Writing – review & editing. LH: Data curation, Resources, Writing – review & editing. NB: Conceptualization, Supervision, Funding acquisition, Writing – review & editing. FT: Conceptualization, Methodology, Formal analysis, Supervision, Writing – original draft.

Competing interests

The authors declare that they have no conflict of interest.

Code and data availability

All data are available as cited in the text from the FLUXNET initiative. The code can be found in the following git repository: `https://gitlab.ethz.ch/ftschurr/longterm_ch-oe2_gpp_paper`

References

Anav, A., Friedlingstein, P., Beer, C., Ciais, P., Harper, A., Jones, C., Murray-Tortarolo, G., Papale, D., Parazoo, N. C., Peylin, P., Piao, S., Sitch, S., Viovy, N., Wiltshire, A., and Zhao, M.: Spatiotemporal patterns of terrestrial gross primary production: A review. *Reviews of Geophysics* 53.3. Publisher: John Wiley & Sons, Ltd, pp. 785–818. DOI: 10.1002/2015RG000483, 2015.

Anthoni, P. M., Freibauer, A., Kolle, O., and Schulze, E.-D.: Winter wheat carbon exchange in Thuringia, Germany. *Agricultural and Forest Meteorology* 121.1, pp. 55–67. DOI: 10.1016/S0168-1923(03)00162-X, 2004.

Asseng, S., Ewert, F., Martre, P., Rötter, R., Lobell, D., Cammarano, D., Kimball, B., Ottman, M., Wall, G., White, J., Reynolds, M., Alderman, P., Prasad, P., Aggarwal, P., Anothai, J., Basso, B., Biernath, C., Challinor, A., De Sanctis, G., Doltra, J., Fereres, E., Garcia-Vile, M., Gayler, S., Hoogenboom, G., Hunt, L., Izaurralde, R., Jabloun, M., Jones, C., Kersebaum, K., Koehler, A., Müller, C., Kumar, S., Nendel, C., O'Leary, G., Olesen, J., Palosuo, T., Priesack, E., Rezaei, E., Ruane, A., Semenov, M., Shcherbak, I., Stöckle, C., Stratonovitch, P., Streck, T., Supit, I., Tao, F., Thorburn, P., Waha, K., Wang, E., Wallach, D., Wolf, I., Zhao, Z., and Zhu, Y.: Rising temperatures reduce global wheat production. *Nature Climate Change* 5.2, pp. 143–147. DOI: 10.1038/NCLIMATE2470, 2015.

Aubinet, M., Moureaux, C., Bodson, B., Dufranne, D., Heinesch, B., Suleau, M., Vancutsem, F., and Vilret, A.: Carbon sequestration by a crop over a 4-year sugar beet/winter wheat/seed potato/winter wheat rotation cycle. *Agricultural and Forest Meteorology* 149.3, pp. 407–418. DOI: 10.1016/j.agrformet.2008.09.003, 2009.

Balsamo, G., Albergel, C., Beljaars, A., Boussetta, S., Brun, E., Cloke, H., Dee, D., Dutra, E., Muñoz-Sabater, J., Pappenberger, F., Rosnay, P. de, Stockdale, T., and Vitart, F.: ERA-Interim/Land: a global land surface reanalysis data set. *Hydrology and Earth System Sciences* 19.1. Publisher: Copernicus Publications, pp. 389–407. DOI: 10.5194/hess-19-389-2015, 2015.

Bates, D., Mächler, M., Bolker, B., and Walker, S.: Fitting linear mixed-effects models using lme4. *Journal of Statistical Software* 67.1, pp. 1–48. DOI: 10.18637/jss.v067.i01, 2015.

Beguería, S. and Vicente-Serrano, S. M.: *SPEI: Calculation of the standardized precipitation-evapotranspiration index*. R package version 1.8.1. URL: https://CRAN.R-project.org/package=SPEI, 2023.

Bennett, A. C., Arndt, S. K., Bennett, L. T., Knauer, J., Beringer, J., Griebel, A., Hinko-Najera, N., Liddell, M. J., Metzen, D., Pendall, E., Silberstein, R. P., Wardlaw, T. J., Woodgate, W., and Haverd, V.: Thermal optima of gross primary productivity are closely aligned with mean air temperatures across Australian wooded ecosystems. *Global Change Biology* 27.19. Publisher: John Wiley & Sons, Ltd, pp. 4727–4744. DOI: 10.1111/gcb.15760, 2021.

Bernacchi, C. J., Singsaas, E. L., Pimentel, C., Portis Jr, A. R., and Long, S. P.: Improved temperature response functions for models of Rubisco-limited photosynthesis. *Plant, Cell & Environment* 24.2. Publisher: John Wiley & Sons, Ltd, pp. 253–259. DOI: 10.1111/j.1365-3040.2001.00668.x, 2001.

Béziat, P., Ceschia, E., and Dedieu, G.: Carbon balance of a three crop succession over two cropland sites in South West France. *Agricultural and Forest Meteorology* 149.10, pp. 1628–1645. DOI: 10.1016/j.agrformet.2009.05.004, 2009.

Bonan, G.: Forests and climate change: Forcings, feedbacks, and the climate benefits of forests. *Science* 320.5882, pp. 1444–1449. DOI: 10.1126/science.1155121, 2008.

Borowiec, M. L., Dikow, R. B., Frandsen, P. B., McKeeken, A., Valentini, G., and White, A. E.: Deep learning as a tool for ecology and evolution. *Methods in Ecology and Evolution* 13.8. Publisher: John Wiley & Sons, Ltd, pp. 1640–1660. DOI: 10.1111/2041-210X.13901, 2022.

Buchmann, N., Hortnagl, L., Keller, S., and Turco, F.: *Fluxnet Product from Oensingen crop, 2003-12-31–2023-12-31.* URL: https://hdl.handle.net/11676/lWly2Cb3xiVw8QB-Z1SXWqKx, 2024.

Buysse, P., Bodson, B., Debacq, A., Ligne, A. D., Heinesch, B., Manise, T., Moureaux, C., and Aubinet, M.: Carbon budget measurement over 12 years at a crop production site in the silty-loam region in Belgium. *Agricultural and Forest Meteorology* 246, pp. 241–255. DOI: 10.1016/j.agrformet.2017.07.004, 2017.

Cai, L., Kreft, H., Taylor, A., Denelle, P., Schrader, J., Essl, F., Kleunen, M. van, Pergl, J., Pyšek, P., Stein, A., Winter, M., Barcelona, J. F., Fuentes, N., Inderjit, Karger, D. N., Kartesz, J., Kuprijanov, A., Nishino, M., Nickrent, D., Nowak, A., Patzelt, A., Pelser, P. B., Singh, P., Wieringa, J. J., and Weigelt, P.: Global models and predictions of plant diversity based on advanced machine learning techniques. *New Phytologist* 237.4. Publisher: John Wiley & Sons, Ltd, pp. 1432–1445. DOI: 10.1111/nph.18533, 2023.

Ceschia, E., Béziat, P., Dejoux, J., Aubinet, M., Bernhofer, C., Bodson, B., Buchmann, N., Carrara, A., Cellier, P., Di Tommasi, P., Elbers, J., Eugster, W., Grünwald, T., Jacobs, C., Jans, W., Jones, M., Kutsch, W., Lanigan, G., Magliulo, E., Marloie, O., Moors, E., Moureaux, C., Olioso, A., Osborne, B., Sanz, M., Saunders, M., Smith, P., Soegaard, H., and Wattenbach, M.: Management effects on net ecosystem carbon and GHG budgets at European crop sites. *The carbon balance of European croplands* 139.3, pp. 363–383. DOI: 10.1016/j.agee.2010.09.020, 2010.

Chen, H., Bai, X., Li, Y., Li, Q., Wu, L., Chen, F., Li, C., Deng, Y., Xi, H., Ran, C., Luo, X., and Liu, M.: Soil drying weakens the positive effect of climate factors on global gross primary production. *Ecological Indicators* 129, p. 107953. DOI: 10.1016/j.ecolind.2021.107953, 2021.

Chen, H., Covert, I. C., Lundberg, S. M., and Lee, S.-I.: Algorithms to estimate Shapley value feature attributions. en. *Nature Machine Intelligence* 5.6. Number: 6 Publisher: Nature Publishing Group, pp. 590–601. DOI: 10.1038/s42256-023-00657-x, 2023.

Chen, T., He, T., Benesty, M., Khotilovich, V., Tang, Y., Cho, H., Chen, K., Mitchell, R., Cano, I., Zhou, T., Li, M., Xie, J., Lin, M., Geng, Y., Li, Y., and Yuan, J.: *XGBoost: Extreme Gradient Boosting.* R package version 1.7.6.1. URL: https://CRAN.R-project.org/package=xgboost, 2023.

Chen, Y., Feng, X., Tian, H., Wu, X., Gao, Z., Feng, Y., Piao, S., Lv, N., Pan, N., and Fu, B.: Accelerated increase in vegetation carbon sequestration in China after 2010: A turning point resulting from climate and human interaction. *Global Change Biology* 27.22, pp. 5848–5864. DOI: 10.1111/gcb.15854, 2021.

Deryng, D., Conway, D., Ramankutty, N., Price, J., and Warren, R.: Global crop yield response to extreme heat stress under multiple climate change futures. *Environmental Research Letters* 9.3. ISBN: 1748-9326 Publisher: IOP Publishing, p. 034011. DOI: 10.1088/1748-9326/9/3/034011, 2014.

Dietiker, D., Buchmann, N., and Eugster, W.: Testing the ability of the DNDC model to predict CO_2 and water vapour fluxes of a Swiss cropland site. *The carbon balance of European croplands* 139.3, pp. 396–401. DOI: 10.1016/j.agee.2010.09.002, 2010.

Dold, C., Büyükcangaz, H., Rondinelli, W., Prueger, J., Sauer, T., and Hatfield, J.: Long-term carbon uptake of agro-ecosystems in the Midwest. *Agricultural and Forest Meteorology* 232, pp. 128–140. DOI: 10.1016/j.agrformet.2016.07.012, 2017.

Eichelmann, E., Wagner-Riddle, C., Warland, J., Deen, B., and Voroney, P.: Carbon dioxide exchange dynamics over a mature switchgrass stand. *Global Change Biology Bioenergy* 8.2. _eprint: https://onlinelibrary.wiley.com/doi/pdf/10.1111/gcbb.12259, pp. 428–442. DOI: 10.1111/gcbb.12259, 2016.

Elzhov, T. V., Mullen, K. M., Spiess, A.-N., and Bolker, B.: *minpack.lm: R Interface to the Levenberg-Marquardt Nonlinear Least-Squares Algorithm Found in MINPACK, Plus Support for Bounds.* R package version 1.2-4. URL: https://CRAN.R-project.org/package=minpack.lm, 2023.

Emmel, C., Winkler, A., Hörtnagl, L., Revill, A., Ammann, C., D'Odorico, P., Buchmann, N., and Eugster, W.: Integrated management of a Swiss cropland is not sufficient to preserve its soil carbon pool in the long term. *Biogeosciences* 15.17, pp. 5377–5393. DOI: 10.5194/bg-15-5377-2018, 2018.

Falge, E., Baldocchi, D., Tenhunen, J., Aubinet, M., Bakwin, P., Berbigier, P., Bernhofer, C., Burba, G., Clement, R., Davis, K. J., Elbers, J. A., Goldstein, A. H., Grelle, A., Granier, A., Gumundsson, J., Hollinger, D., Kowalski, A. S., Katul, G., Law, B. E., Malhi, Y., Meyers, T., Monson, R. K., Munger, J., Oechel, W., Paw U, K. T., Pilegaard, K., Rannik, Ü., Rebmann, C., Suyker, A., Valentini, R., Wilson, K., and Wofsy, S.: Seasonality of ecosystem respiration and gross primary production as derived from FLUXNET measurements. *FLUXNET 2000 Synthesis* 113.1, pp. 53–74. DOI: 10.1016/S0168-1923(02)00102-8, 2002.

FAO: *Land use statistics and indicators 2000–2021: Global, regional and country trends.* FAOSTAT Analytical Briefs Series 71. Rome: Food and Agriculture Organization of the United Nations. DOI: 10.4060/cc6907en. URL: https://doi.org/10.4060/cc6907en, 2023.

Guevara-Escobar, A., González-Sosa, E., Cervantes-Jiménez, M., Suzán-Azpiri, H., Queijeiro-Bolaños, M. E., Carrillo-Ángeles, I., and Cambrón-Sandoval, V. H.: Machine learning estimates of eddy covariance carbon flux in a scrub in the Mexican highland. *Biogeosciences* 18.2. Publisher: Copernicus Publications, pp. 367–392. DOI: 10.5194/bg-18-367-2021, 2021.

Hastings, A. F., Wattenbach, M., Eugster, W., Li, C., Buchmann, N., and Smith, P.: Uncertainty propagation in soil greenhouse gas emission models: An experiment using the DNDC model and at the Oensingen cropland site. *Agriculture, Ecosystems & Environment* 136.1, pp. 97–110. DOI: 10.1016/j.agee.2009.11.016, 2010.

Holzkämper, A., Fossati, D., Hiltbrunner, J., and Fuhrer, J.: Spatial and temporal trends in agro-climatic limitations to production potentials for grain maize and winter wheat in Switzerland. *Regional Environmental Change* 15.1, pp. 109–122. DOI: 10.1007/s10113-014-0627-7, 2015.

Huang, M., Piao, S., Ciais, P., Peñuelas, J., Wang, X., Keenan, T. F., Peng, S., Berry, J. A., Wang, K., Mao, J., Alkama, R., Cescatti, A., Cuntz, M., De Deurwaerder, H., Gao, M., He, Y., Liu, Y., Luo, Y., Myneni, R. B., Niu, S., Shi, X., Yuan, W., Verbeeck, H., Wang, T., Wu, J., and Janssens, I. A.: Air temperature optima of vegetation productivity across global biomes. *Nature Ecology & Evolution* 3.5, pp. 772–779. DOI: 10.1038/s41559-019-0838-x, 2019.

Krebs, L., Hörtnagl, L., Scapucci, L., Gharun, M., Feigenwinter, I., and Buchmann, N.: Net ecosystem CO_2 exchange of a subalpine spruce forest in Switzerland over 26 years: Effects of phenology and contributions of abiotic drivers at daily time scales. *Global Change Biology* 31.7. Publisher: John Wiley & Sons, Ltd, p. 70371. DOI: 10.1111/gcb.70371, 2025.

Le Roux, R., Furusho-Percot, C., Deswarte, J.-C., Bancal, M.-O., Chenu, K., Noblet-Ducoudré, N. de, Cortázar-Atauri, I. G. de, Durand, A., Bulut, B., Maury, O., Décome, J., and Launay, M.: Mapping the race between crop phenology and climate risks for wheat in France under climate change. *Scientific Reports* 14.1, p. 8184. DOI: 10.1038/s41598-024-58826-w, 2024.

Li, M., Zhu, Z., Ren, W., and Wang, Y.: Predicting gross primary productivity under future climate change for the tibetan plateau based on convolutional neural networks. *Remote Sensing* 16.19, p. 3723. DOI: 10.3390/rs16193723, 2024.

Liu, F., Zhang, Y., Wang, X., Qi, Y., Min, L., Yu, G., Hu, C., and Shen, Y.: Achieving grain security and carbon neutrality: Challenges from carbon allocation. *Journal of Cleaner Production* 427, p. 139214. DOI: 10.1016/j.jclepro.2023.139214, 2023.

Liu, L., Zhou, W., Guan, K., Peng, B., Xu, S., Tang, J., Zhu, Q., Till, J., Jia, X., Jiang, C., Wang, S., Qin, Z., Kong, H., Grant, R., Mezbahuddin, S., Kumar, V., and Jin, Z.: Knowledge-guided machine learning can improve carbon cycle quantification in agroecosystems. *Nature Communications* 15.1, p. 357. DOI: 10.1038/s41467-023-43860-5, 2024.

Liu, Y. and Just, A.: *SHAPforxgboost: SHAP plots for 'XGBoost'*. R package version 0.1.3. URL: https://CRAN.R-project.org/package=SHAPforxgboost, 2023.

Liu, Y., Chen, Q., Ge, Q., Dai, J., Qin, Y., Dai, L., Zou, X., and Chen, J.: Modelling the impacts of climate change and crop management on phenological trends of spring and winter wheat in China. *Agricultural and Forest Meteorology* 248, pp. 518–526. DOI: 10.1016/j.agrformet.2017.09.008, 2018.

Lu, Q., Liu, H., Wei, L., Zhong, Y., and Zhou, Z.: Global prediction of gross primary productivity under future climate change. *Science of the Total Environment* 912, p. 169239. DOI: 10.1016/j.scitotenv.2023.169239, 2024.

Lundberg, S. and Lee, S.-I.: *A unified approach to interpreting model predictions*. DOI: 10.48550/arXiv.1705.07874, 2017.

Menefee, D., Lee, T., Flynn, K., Chen, J., Abraha, M., Baker, J., and Suyker, A.: Machine learning algorithms improve MODIS GPP estimates in United States croplands. *Frontiers in Remote Sensing* 4. DOI: 10.3389/frsen.2023.1240895, 2023.

https://doi.org/10.5194/egusphere-2026-5253
Preprint. Discussion started: 11 September 2026

MeteoSwiss and Zurich, E.: *Climate CH2025 - Scientific Report*. Tech. rep. Zurich: Federal Office of Meteorology and Climatology MeteoSwiss. DOI: `10.18751/climate/scenarios/ch2025/sr/1.0/`. URL: `https://doi.org/10.18751/climate/scenarios/ch2025/sr/1.0/`, 2025.

Moureaux, C., Debacq, A., Hoyaux, J., Suleau, M., Tourneur, D., Vancutsem, F., Bodson, B., and Aubinet, M.: Carbon balance assessment of a Belgian winter wheat crop (Triticum aestivum L.) *Global Change Biology* 14.6. ISBN: 1354-1013 Publisher: Wiley Online Library, pp. 1353–1366. DOI: `10.1111/j.1365-2486.2008.01560.x`, 2008.

Niedziński, T., Sierra, M. J., Łabętowicz, J., Noras, K., Cabrales, C., and Millán, R.: Release of nitrogen from granulate mineral and organic fertilizers and its effect on selected chemical parameters of soil. *Agronomy* 11.10, p. 1981. DOI: `10.3390/agronomy11101981`, 2021.

Pan, L., Xiao, X., Yao, Y., Pan, B., Yin, C., Meng, C., Qin, Y., and Zhang, C.: Site-specific apparent optimum air temperature for vegetation photosynthesis across the globe. *Scientific Data* 11.1, p. 758. DOI: `10.1038/s41597-024-03603-7`, 2024.

Papale, D., Reichstein, M., Aubinet, M., Canfora, E., Bernhofer, C., Kutsch, W., Longdoz, B., Rambal, S., Valentini, R., Vesala, T., and Yakir, D.: Towards a standardized processing of Net Ecosystem Exchange measured with eddy covariance technique: algorithms and uncertainty estimation. English. *Biogeosciences* 3.4. Publisher: Copernicus GmbH, pp. 571–583. DOI: `10.5194/bg-3-571-2006`, 2006.

Pastorello, G. et al.: The FLUXNET2015 dataset and the ONEFlux processing pipeline for eddy covariance data. *Scientific Data* 7.1, p. 225. DOI: `10.1038/s41597-020-0534-3`, 2020.

Pichler, M. and Hartig, F.: Machine learning and deep learning—A review for ecologists. *Methods in Ecology and Evolution* 14.4. Publisher: John Wiley & Sons, Ltd, pp. 994–1016. DOI: `10.1111/2041-210X.14061`, 2023.

Porter, J. R. and Gawith, M.: Temperatures and the growth and development of wheat: a review. *European Journal of Agronomy* 10.1, pp. 23–36. DOI: `10.1016/S1161-0301(98)00047-1`, 1999.

Reichstein, M., Falge, E., Baldocchi, D., Papale, D., Aubinet, M., Berbigier, P., Bernhofer, C., Buchmann, N., Gilmanov, T., Granier, A., Grünwald, T., Havránková, K., Ilvesniemi, H., Janous, D., Knohl, A., Laurila, T., Lohila, A., Loustau, D., Matteucci, G., Meyers, T., Miglietta, F., Ourcival, J.-M., Pumpanen, J., Rambal, S., Rotenberg, E., Sanz, M., Tenhunen, J., Seufert, G., Vaccari, F., Vesala, T., Yakir, D., and Valentini, R.: On the separation of net ecosystem exchange into assimilation and ecosystem respiration: review and improved algorithm. *Global Change Biology* 11.9. _eprint: https://onlinelibrary.wiley.com/doi/pdf/10.1111/j.1365-2486.2005.001002.x, pp. 1424–1439. DOI: `10.1111/j.1365-2486.2005.001002.x`, 2005.

Rezaei, E., Siebert, S., Hüging, H., and Ewert, F.: Climate change effect on wheat phenology depends on cultivar change. *Scientific Reports* 8, p. 4891. DOI: `10.1038/s41598-018-23101-2`, 2018.

Scapucci, L., Shekhar, A., Aranda-Barranco, S., Bolshakova, A., Hörtnagl, L., Gharun, M., and Buchmann, N.: Compound soil and atmospheric drought (CSAD) events and CO_2 fluxes of a mixed deciduous forest: the occurrence, impact, and temporal contribution of main drivers. *Biogeosciences* 21.15. Publisher: Copernicus Publications, pp. 3571–3592. DOI: `10.5194/bg-21-3571-2024`, 2024.

Schils, R. L., Bufe, C., Rhymer, C. M., Francksen, R. M., Klaus, V. H., Abdalla, M., Milazzo, F., Lellei-Kovács, E., Berge, H. t., Bertora, C., Chodkiewicz, A., Dămătîrcă, C., Feigenwinter, I., Fernández-Rebollo, P., Ghiasi, S., Hejduk, S., Hiron, M., Janicka, M., Pellaton, R., Smith, K. E., Thorman, R., Vanwalleghem, T., Williams, J., Zavattaro, L., Kampen, J., Derkx, R., Smith, P., Whittingham, M. J., Buchmann, N., and Price, J. P. N.: Permanent grasslands in Europe: Land use change and intensification decrease their multifunctionality. *Agriculture, Ecosystems & Environment* 330, p. 107891. DOI: 10.1016/j.agee.2022.107891, 2022.

Schmidt, M., Reichenau, T., Fiener, P., and Schneider, K.: The carbon budget of a winter wheat field: An eddy covariance analysis of seasonal and inter-annual variability. *Agricultural and Forest Meteorology* 165, pp. 114–126. DOI: 10.1016/j.agrformet.2012.05.012, 2012.

Snoek, J., Larochelle, H., and Adams, R. P.: Practical bayesian optimization of machine learning algorithms. *Advances in Neural Information Processing Systems* 25. DOI: 10.48550/arXiv.1206.2944, 2012.

Supit, I., Diepen, C. van, Wit, A. de, Kabat, P., Baruth, B., and Ludwig, F.: Recent changes in the climatic yield potential of various crops in Europe. *Agricultural Systems* 103.9, pp. 683–694. DOI: 10.1016/j.agsy.2010.08.009, 2010.

Suyker, A. E., Verma, S. B., Burba, G. G., and Arkebauer, T. J.: Gross primary production and ecosystem respiration of irrigated maize and irrigated soybean during a growing season. *Agricultural and Forest Meteorology* 131.3, pp. 180–190. DOI: 10.1016/j.agrformet.2005.05.007, 2005.

SwissFluxNet: *Oensingen Site Information*. https://www.swissfluxnet.ethz.ch/index.php/sites/site-info-ch-oe2/. Accessed: 2026-01-15, accessed 2026.

Trnka, M., Rötter, R., Ruiz-Ramos, M., Kersebaum, K., Olesen, J., Zalud, Z., and Semenov, M.: Adverse weather conditions for European wheat production will become more frequent with climate change. *Nature Climate Change* 4.7, pp. 637–643. DOI: 10.1038/NCLIMATE2242, 2014.

Tschurr, F., Roth, L., Storni, N., Zumsteg, O., Walter, A., and Anderegg, J.: Temporal resolution trumps spectral resolution in UAV-based monitoring of cereal senescence dynamics. en. *Plant Methods* 20.1, p. 188. DOI: 10.1186/s13007-024-01308-x, 2024.

Wang, H., Shao, W., Hu, Y., Cao, W., and Zhang, Y.: Assessment of six machine learning methods for predicting gross primary productivity in grassland. *Remote Sensing* 15.14, p. 3475. DOI: 10.3390/rs15143475, 2023.

Wang, X., Jin, Y., Schmitt, S., and Olhofer, M.: Recent advances in bayesian optimization. *ACM Computing Surveys* 55.13S. DOI: 10.1145/3582078, 2023.

Wang, Y., Feigenwinter, I., Hörtnagl, L., Gilgen, A. K., and Buchmann, N.: Drivers of long-term grassland CO_2 fluxes: effects of management and meteorological conditions during regrowth periods. English. *Biogeosciences* 23.4. Publisher: Copernicus GmbH, pp. 1625–1652. DOI: 10.5194/bg-23-1625-2026, 2026.

Wu, J., Chen, X.-Y., Zhang, H., Xiong, L.-D., Lei, H., and Deng, S.-H.: Hyperparameter optimization for machine learning models based on bayesian optimization. *Journal of Electronic Science and Technology* 17.1, pp. 26–40. DOI: 10.11989/JEST.1674-862X.80904120, 2019.

Xiao, D., Tao, F., Liu, Y., Shi, W., Wang, M., Liu, F., Zhang, S., and Zhu, Z.: Observed changes in winter wheat phenology in the North China Plain for 1981-2009. *International Journal of Biometeorology* 57.2, pp. 275–285. DOI: 10.1007/s00484-012-0552-8, 2013.

Xu, D., Zhu, Y., Zhu, H., Hu, Q., Liu, G., Wei, H., and Zhang, H.: Effects of a one-time application of controlled-release nitrogen fertilizer on yield and nitrogen accumulation and utilization of late japonica rice in China. *Agriculture* 11.11, p. 1041. DOI: 10.3390/agriculture11111041, 2021.

Zhang, Q., Lei, H., Yang, D., Xiong, L., Liu, P., and Fang, B.: Decadal variation in CO_2 fluxes and its budget in a wheat and maize rotation cropland over the North China Plain. *Biogeosciences* 17.8. Publisher: Copernicus Publications, pp. 2245–2262. DOI: 10.5194/bg-17-2245-2020, 2020.

Zhang, Y., Song, C., Band, L. E., and Sun, G.: No proportional increase of terrestrial gross carbon sequestration from the greening Earth. *Journal of Geophysical Research: Biogeosciences* 124.8. Publisher: John Wiley & Sons, Ltd, pp. 2540–2553. DOI: 10.1029/2018JG004917, 2019.

Zhao, Y., Wang, L., Jiang, Q., and Wang, Z.: Sensitivity of gross primary production to precipitation and the driving factors in China's agricultural ecosystems. *Science of The Total Environment* 948, p. 174938. DOI: 10.1016/j.scitotenv.2024.174938, 2024.

Zhou, B., Chen, G., Yu, H., Zhao, J., and Yin, Y.: Revealing the nonlinear impact of human activities and climate change on ecosystem services in the karst region of southeastern yunnan using the XGBoost–SHAP model. *Forests* 15.8. ISBN: 1999-4907 Publisher: MDPI, p. 1420. DOI: 10.3390/f15081420, 2024.

Zhu, Z., Piao, S., Myneni, R. B., Huang, M., Zeng, Z., Canadell, J. G., Ciais, P., Sitch, S., Friedlingstein, P., Arneth, A., Cao, C., Cheng, L., Kato, E., Koven, C., Li, Y., Lian, X., Liu, Y., Liu, R., Mao, J., Pan, Y., Peng, S., Peñuelas, J., Poulter, B., Pugh, T. A. M., Stocker, B. D., Viovy, N., Wang, X., Wang, Y., Xiao, Z., Yang, H., Zaehle, S., and Zeng, N.: Greening of the Earth and its drivers. *Nature Climate Change* 6.8, pp. 791–795. DOI: 10.1038/nclimate3004, 2016.

https://doi.org/10.5194/egusphere-2026-5253
Preprint. Discussion started: 11 September 2026

A Supplementary Materials

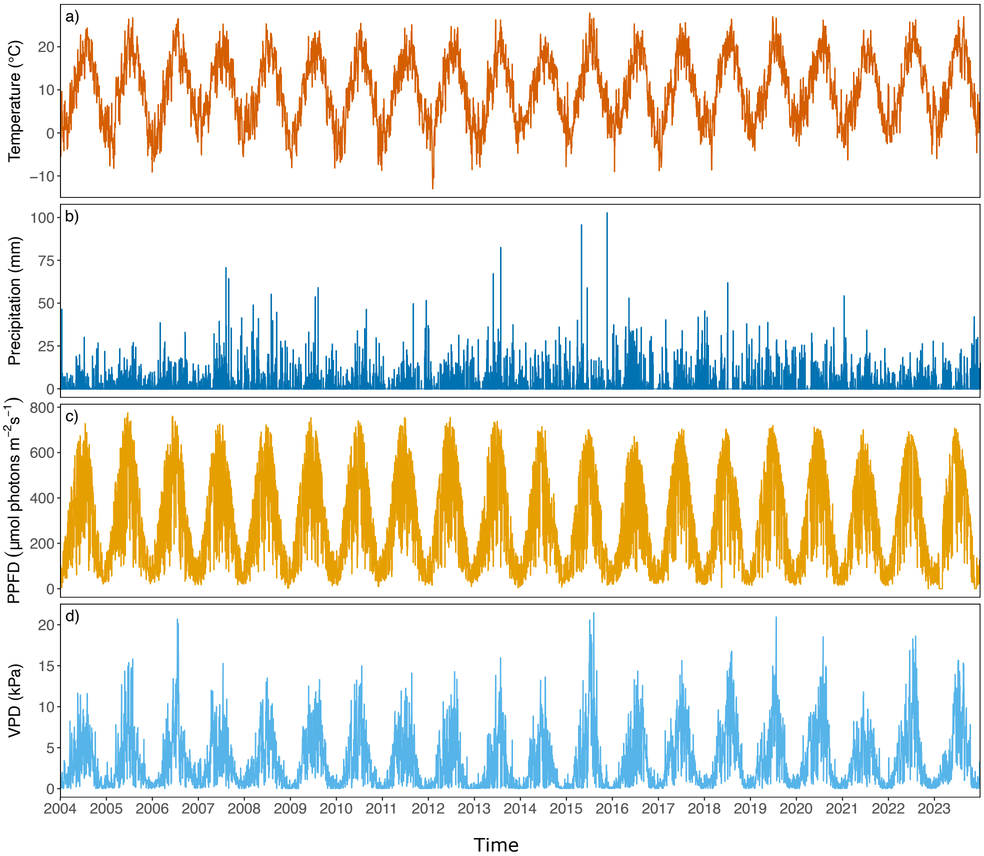

Figure A.1: Daily values of the climatic variables — namely temperature (a), precipitation (b), PPFD (c), and VPD (d) — over the study period (2004-2023).

https://doi.org/10.5194/egusphere-2026-5253
Preprint. Discussion started: 11 September 2026

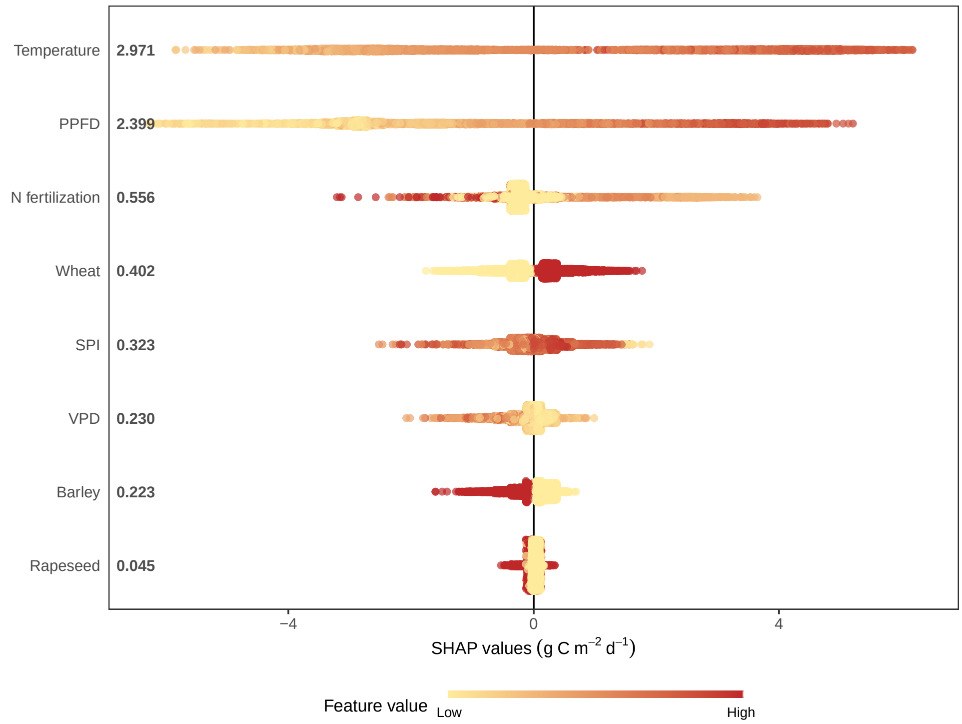

Figure A.2: SHAP summary plot showing the importance of predictors in the XGBoost model for the first model (data after the end of the main growing season excluded). The x-axis shows the SHAP values for each observation, and colors indicate the actual variable value (red = high, yellow = low). The mean SHAP value for each variable, shown on the right, represents its average contribution to the model predictions over the study period. The 0 values represent the baseline of the SHAP analysis with a value of 6.55 g C m^{-2} d^{-1}.

https://doi.org/10.5194/egusphere-2026-5253
Preprint. Discussion started: 11 September 2026

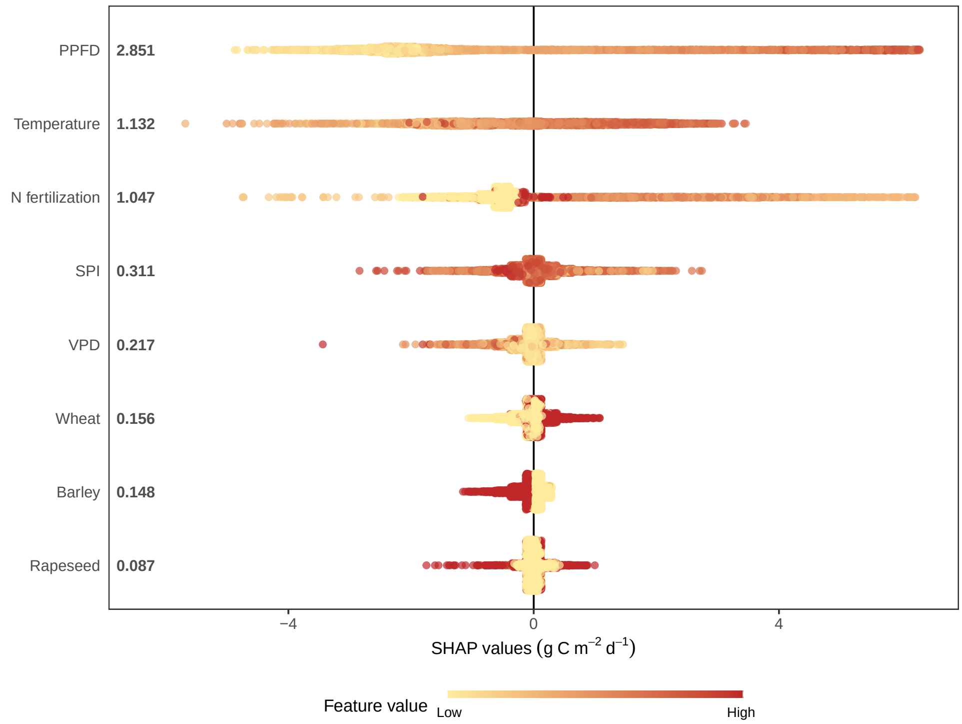

Figure A.3: SHAP summary plot showing the importance of predictors in the XGBoost model for the first model (the whole growing season is used). The x-axis shows the SHAP values for each observation, and colors indicate the actual variable value (red = high, yellow = low). The mean SHAP value for each variable, shown on the right, represents its average contribution to the model predictions over the study period. The 0 values represent the baseline of the SHAP analysis with a value of $4.59\,\mathrm{g\,C\,m^{-2}\,d^{-1}}$.

https://doi.org/10.5194/egusphere-2026-5253
Preprint. Discussion started: 11 September 2026

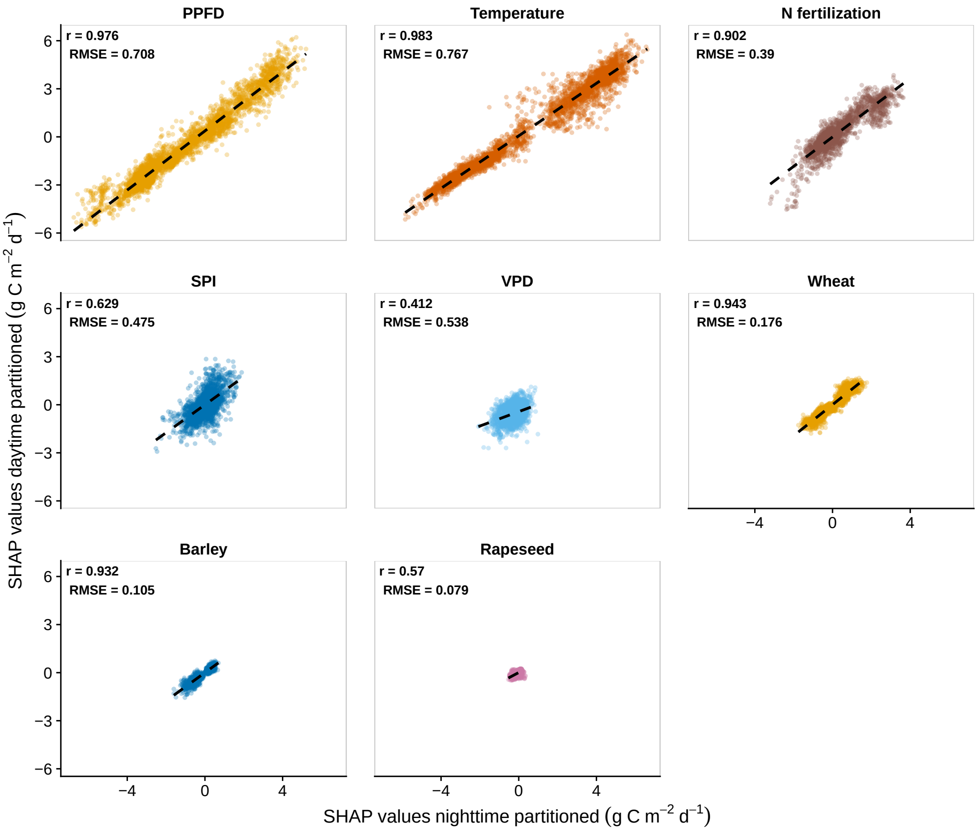

Figure A.4: Scatter plots compare feature contributions (SHAP values) derived from nighttime-partitioned (*GPP_NT_CUT_50*) and daytime-partitioned (*GPP_DT_CUT_50*) models. Each panel represents a specific predictor, with the dashed line indicating the linear fit. Pearson correlation coefficients (r) and Root Mean Square Error ($RMSE$) are displayed in the upper-left corner of each facet.

https://doi.org/10.5194/egusphere-2026-5253
Preprint. Discussion started: 11 September 2026

Table A.1: Crop rotation at the study site over the investigation period, showing the cultivated crop for each season along with the corresponding sowing and harvest dates. Nitrogen fertilization for each growing season is reported as the cumulative N input over the season.

Crop	Sowing date	Harvest date	Total N applied (kg N ha^{-1})
Winter Wheat	16 Oct 2003	04 Aug 2004	127
Winter Barley	29 Sep 2004	14 Jul 2005	100.5
Cover crop	09 Aug 2005		0
Potato	05 May 2006		0
Winter Wheat	19 Oct 2006	15 Jul 2007	140
Winter Rapeseed	28 Aug 2007	16 Jul 2008	161.5
Winter Wheat	07 Oct 2008	21 Jul 2009	116
Cover crop	12 Aug 2009	0	
Peas	09 May 2010	19 Jul 2010	0
Winter Wheat	15 Oct 2010	02 Aug 2011	157.5
Winter Barley	24 Sep 2011	09 Jul 2012	87
Winter Rapeseed	04 Sep 2012	28 Jul 2013	144
Winter Wheat	19 Oct 2013	24 Jul 2014	124
Winter Barley	29 Sep 2014	04 Jul 2015	115
Cover crop	03 Aug 2015		0
Peas	09 May 2016	25 Jul 2016	0
Winter Wheat	12 Oct 2016	19 Jul 2017	154.1
Winter Rapeseed	30 Aug 2017	12 Jul 2018	171
Winter Wheat	11 Oct 2018	19 Jul 2019	136
Winter Barley	04 Oct 2019	01 Jul 2020	48
Grass	03 Apr 2020	19 Oct 2020	
Grass-Clover	19 Aug 2020	19 Oct 2020	
Grass-Clover		30 May 2021	
Grass-Clover		20 Jul 2021	
Grass-Clover		02 Sep 2021	
Grass-Clover		18 Oct 2021	
Grass-Clover		14 May 2022	
Grass-Clover		25 Jun 2022	
Grass-Clover		08 Aug 2022	
Grass-Clover		20 Sep 2022	
Winter Wheat	06 Oct 2022	15 Jul 2023	137.7
Cover crop	27 Jul 2023	25 Sep 2023	
Winter Barley	04 Oct 2023	04 Jul 2024	

Table A.2: Results of linear models of annual data between environmental covariates (vapor pressure deficit (VPD; kPa), precipitation (mm), air temperature (°C), and radiation (PPFD; μmol photons m^{-2}s^{-1}) and time. *Note:* $^{*}p < 0.1$, $^{**}p < 0.05$, $^{***}p < 0.01$.

Variable	Slope	P value	Significance
VPD	0.04424	0.02764	*
precipitation	5.07812	0.43972	
Air temperature	0.06363	0.02484	*
PPFD	-0.85408	0.12824	

https://doi.org/10.5194/egusphere-2026-5253
Preprint. Discussion started: 11 September 2026

Table A.3: Results of linear mixed effect models of seasonal data between environmental covariates (vapor pressure deficit (VPD; kPa), precipitation (P; mm), air temperature (TA; °C), and radiation (PPFD; μmol photons $m^{-2}s^{-1}$) and time with crop type as a random factor. *Note:* $^{*}p < 0.1$, $^{**}p < 0.05$, $^{***}p < 0.01$.

Variable	Slope	P value	Significance
VPD	0.02355	0.48278	
P	-2.76644	0.66859	
TA	0.10213	0.22738	
PPFD	-1.92919	0.29171	

Table A.4: Results of linear mixed effect models of management data (sowing and harvest dates) over the years with the crop type as random factor. *Note:* $^{*}p < 0.1$, $^{**}p < 0.05$, $^{***}p < 0.01$.

Variable	Slope	P Value	Significance
Sowing date	-0.07	0.726	
Harvest date	-0.647	0.012	*

Table A.5: Linear regression trends of environmental covariates during the fixed growing season (October–July) and post-harvest off-season (August–September). Slopes represent average annual changes over the study period. Variables include vapor pressure deficit (VPD), precipitation (P), air temperature (T_a), and photosynthetic photon flux density (PPFD). Asterisks denote statistical significance (** $p < 0.05$, *** $p < 0.01$).

		Growing Season (Oct–Jul)			**Off Season (Aug–Sep)**		
Variable	**Units**	**Slope**	**P Value**	**Significance**	**Slope**	**P Value**	**Significance**
VPD	kPa	-0.008	0.717		0.130	0.003	***
P	mm	2.618	0.742		-3.479	0.214	
TA	°C	0.010	0.749		0.081	0.035	**
PPFD	μmol photons m^{-2} s^{-1}	-3.807	0.005	***	0.451	0.620	

Table A.6: Linear model outputs of GPP cumulative max per season and Harvest Index (unitless), Total Harvest (kg ha^{-1}), Straw Harvest (kg ha^{-1}), and Grain Harvest (kg ha^{-1}) with the winter wheat and winter barley data (see Figure 5).*Note:* $^{*}p < 0.1$, $^{**}p < 0.05$, $^{***}p < 0.01$.

	Variable	Slope	P Value	Significance
1	Harvest Index	-0.00038	0.01983	*
2	Total Harvest	6.61801	0.00199	**
3	Straw Harvest	5.6638	0.00634	**
4	Grain Harvest	0.95421	0.58203	

https://doi.org/10.5194/egusphere-2026-5253
Preprint. Discussion started: 11 September 2026

Table A.7: Search bounds used for Bayesian optimization of XGBoost hyperparameters. The table lists each hyperparameter along with its lower and upper limits considered during the optimization process.

Parameter	Lower bound	Upper bound
max_depth	3	9
eta	0.01	0.3
subsample	0.5	1.0
colsample_bytree	0.5	1.0
min_child_weight	0	10
gamma	0	20
alpha	0	20
lambda	0	20

Table A.8: Hyperparameters of the XGBoost model that are obtained from the Bayesian optimization. Values are shown for the first model (cut), which excludes data after the end of the main growing season, and for the second model (no cut), which is trained on the entire growing season.

Parameters	Value $\text{model}_{\text{cut}}$	Value $\text{model}_{\text{no cut}}$
max_depth	9	8
eta	0.20	0.09
subsample	0.8	0.93
colsample_by_tree	0.98	1
min_child_weight	1.5	1.16
gamma	6.75	0
alpha	0	20
lambda	14.47	20

Table A.9: Skill scores of XGBoost models trained on all crops combined, or individually on wheat, barley, or rapeseed. The models are each time tested on the whole growing season (no cut) or on the growing season before EOS (cut). Metrics reported include the root mean square error (RMSE), mean absolute error (MAE), and the correlation coefficient (r) between predicted and observed GPP values. Scores are given for both the training and testing datasets, with the training set reflecting model fit and the testing set evaluating performance on unseen data.

Model	$\text{RMSE}_{\text{test}}$	$\text{RMSE}_{\text{train}}$	MAE_{test}	$\text{MAE}_{\text{train}}$	cor_{test}	$\text{r}^2{}_{\text{test}}$	$\text{cor}_{\text{train}}$
All crop_{cut}	2.262	1.237	0.113	0.008	0.922	0.851	0.979
All $\text{crop}_{\text{no cut}}$	2.414	1.399	0.099	0.005	0.895	0.801	0.968
$\text{Wheat}_{\text{no cut}}$	2.945	1.847	0.106	0.012	0.876	0.767	0.953
$\text{Barley}_{\text{no cut}}$	2.094	1.633	0.055	0.015	0.896	0.803	0.942
$\text{Rapeseed}_{\text{no cut}}$	2.169	0.689	0.161	0.000	0.868	0.753	0.989
$\text{Wheat}_{\text{cut}}$	2.278	0.917	0.085	0.001	0.941	0.886	0.990
$\text{Barley}_{\text{cut}}$	2.200	1.204	0.013	0.012	0.911	0.830	0.975
$\text{Rapeseed}_{\text{cut}}$	2.127	1.523	0.024	0.030	0.912	0.831	0.955